

# **Development of Corrosion Protection Coating System for Aerospace Grade Aluminum 7075 Alloy**



**By**

**Mohsin Ali Fakhar**

**School of Chemical and Materials Engineering  
National University of Sciences and Technology  
(2023)**

# **Development of Corrosion Protection Coating System for Aerospace Grade Aluminum 7075 Alloy**



Mohsin Ali Fakhar

Regn No: 00000330054

**This thesis is submitted as a partial fulfillment of the requirements for the  
degree of**

**MS in Materials and Surface Engineering**

**Supervisor Name: Dr. Malik Adeel Umer**

**School of Chemical and Materials Engineering (SCME)**

**National University of Sciences and Technology (NUST)**

**H-12 Islamabad, Pakistan**

**November, 2023**



I

THESIS ACCEPTANCE CERTIFICATE

Certified that final copy of MS thesis written by Mr Mohsin Ali Fakhar (Registration No 00000330054), of School of Chemical & Materials Engineering (SCME) has been vetted by undersigned, found complete in all respects as per NUST Statues/Regulations, Is free of plagiarism, errors, and mistakes and is accepted as partial fulfillment for award of MS degree. It is further certified that necessary amendments as pointed out by GEC members of the scholar have also been incorporated in the said thesis.

Signature: \_\_\_\_\_

Name of Supervisor: Dr Malik Adeel Umer

Date: 30-1-2024

Signature (HOD): \_\_\_\_\_

Date: 31.1.2024

Signature (Dean/Principal): \_\_\_\_\_

Date: 31.1.2024



MSE-15-2020

Form TH-1

(Must be type written)

**National University of Sciences & Technology (NUST)****MASTER'S THESIS WORK****Formulation of Guidance and Examination Committee (GEC)**

Name: Mohsin Ali Fakhar

NUST Regn No: 330054

Department: Materials

Specialization: Materials & Surface Engineering

Credit Hour Completed: 24

CGPA: 3.63**Course Work Completed**

S/No	Code	Title	Core/Elective	CH	Grade
1	MSE-821	Mechanical Behaviour Of Materials	Core	3.0	B+
2	RM-898	Research Methodology	Addl	2.0	Q
3	MSE-811	Materials Thermodynamics	Core	3.0	B
4	MSE-881	Manufacturing Processes	Elective	3.0	A
5	MSE-812	Phase Transformation & Microstructures	Core	3.0	C+
6	MSE-851	Surface Engineering & Characterization	Core	3.0	A
7	NSE-842	Nano Materials For Energy Applications	Elective	3.0	A
8	MSE-941	Materials For High Temperature Applications	Elective	3.0	A
9	NSE-961	Surface Coatings and Thin Films	Elective	3.0	A

Date 24-05-2022

Student's Signature

**Thesis Committee**

- Name: Dr. Muhammad Siyar (Supervisor)  
Department: Materials Engineering (SCME)
- Name: Dr. Malik Umer Adeel (Co-Supervisor)  
Department: Materials Engineering (SCME)
- Name: Dr. Mohammad Shahid  
Department: Materials Engineering (SCME)
- Name: Dr. Nasir Muhammad Ahmed  
Department: Materials Engineering (SCME)
- Name: Dr. Laraib Alam Khan (External)  
Department: Composites Division (AWC)-NESCO

Signature:

Signature:

Signature:

Signature:

Signature:

Date: 26/9/2022

Signature of Head of Department:

**APPROVAL**Date: 26-9-2022

Dean/Principal

**Distribution**

1x copy to Exam Branch, Main Office NUST

1x copy to PGP Dte, Main Office NUST

1x copy to Exam branch, respective institute

School of Chemical and Materials Engineering (SCME) Sector H-12, Islamabad



MASTER'S THESIS WORK

We hereby recommend that the dissertation prepared under our supervision by  
Regn No & Name: 00000330054 Mohsin Ali Fakhar

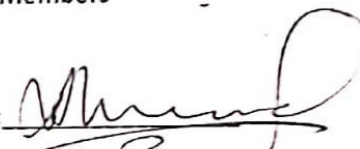
Title: Development of Corrosion Protection Coating System for Aerospace Grade Al-7075 Alloys.

Presented on: 28 Dec 2023 at: 1400 hrs in SCME (Seminar Hall)

Be accepted in partial fulfillment of the requirements for the award of Masters of Science degree in  
**Materials & Surface Engineering.**

Guidance & Examination Committee Members

Name: Dr Nasir M. Ahmed

Signature: 


Name: Dr Muhammad Shahid

Signature: 

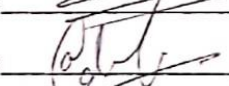
Name: Dr Laralb Alam Khan (External)

Signature: 


Name: Dr Muhammad Syar (Co-Supervisor)


Signature: 

Supervisor's Name: Dr Malik Adeel Umer

Signature: 

Dated: 18/01/24

  
Head of Department  
Date 18.1.24

  
Dean/Principal  
Date 18.1.24

## **DEDICATION**

I dedicate this thesis to my parents as their prayers have always guided me through all the botherations and my beloved wife who always stayed with me in all exasperations of life.

## **ACKNOWLEDGEMENTS**

All admiration to Allah Almighty. He is the One, who bestows and gives the power to us to think, utilize our expertise in knowledge in achieving remarkable solutions for mankind in every field. Therefore, I express my greatest thanks to Almighty Allah the universal and the architect of the world. I like to express my gratefulness to my very supportive and respected supervisor Dr. Malik Umer Adeel for his clear and patient guidance that directed me to fulfill my project and this thesis. His cool and calm behavior motivated me to do my best. His valuable suggestions and feedback contributed to this thesis. Also, I am very grateful to all my GEC members including, Dr. Muhammad Shahid, Dr. Nasir Muhammad Ahmed and Dr. Laraib Alam Khan who helped me and motivated me to do my best. I would also like to thank my parents, family members, and friends for their help, prayers, and their valuable suggestions I want to specifically thank Dr. Muhammad Siyar for co-supervising my project and for his continuous support and motivation which helped me at various stages of my Master's Degree. I am truly grateful to Mr. Basit, Miss Humaira and Mr. Furqan who always abetted me in lab during my research work. I acknowledge the support provided by the Materials Engineering Department of SCME for providing me a platform to perform my experiments and use my skills in research work.

## **Abstract**

Aluminum Alloys are used in Aerospace and Automobile Industries due to their high strength to weight ratio and their ease of formability but there are limitations pertaining to the corrosion protection of the alloys. Presently, Chrome based coatings are applied to Aluminum Alloys but due to their carcinogenic nature, efforts are being made to explore alternates. This work presents the exploration of a potential alternate of Chrome Conversion Coating for the enhancement of corrosion resistance of Al-7075 alloys. Nickel Phosphorus (NiP) based coatings show good corrosion resistance and Boron Nitride (BN) nanoparticles (a refractory material) can be used as an appropriate addition. BN was incorporated in NiP using a simplified coating bath and well optimized parameters. A comparative analysis was carried between BN based NiP and without BN based NiP along with different percentages of BN addition (0.5 ~ 2.0 %). The detailed analysis of the developed coating was carried out via Scanning Electron Microscopy (SEM), Energy Dispersive X-Ray Spectroscopy (EDX), Atomic Force Microscopy (AFM), X-Ray Diffraction (XRD), Nano-Indentation, Micro Hardness, Tafel Scan and Electrochemical Impedance Spectroscopy (EIS). All the results are of the evidence that there is a continuous rise of corrosion protection up to 2.0% and this makes BN as suitable reinforcement for NiP Coating on Aluminum Alloys.



# Table of Contents

Chapter 1 .....	1
Introduction.....	1
1.1 Advance Surface Coating Techniques .....	2
1.2 Significance of the Project .....	2
1.3 Al-7075 -T6 Substrate.....	4
1.4 Corrosion in Al-7075 .....	5
1.5 Corrosion Protection of Al-7075.....	6
1.6 Different Techniques of Electrochemical Deposition .....	10
1.6.1 Electroless Deposition.....	10
1.6.2 Factors Affecting Electroless Bath.....	11
1.6.3 Advantages of Electroless Deposition .....	11
1.7 Electroless Deposition of Nickel Phosphate .....	12
1.8 Aims and Objectives .....	15
1.9 Overall Dissertation Outline .....	15
Chapter 2.....	16
Literature Review.....	16
2.1 Ni-P Coatings.....	17
2.2 Ni-P-Si <sub>3</sub> N <sub>4</sub> Coatings .....	18
2.3 Ni-P-Al <sub>2</sub> O <sub>3</sub> .....	19
2.4 Ni-P-SiC.....	19
2.5 Ni-P-SiO <sub>2</sub> .....	19
2.6 Ni-P-ZnO .....	20
2.7 Ni-P-TiN .....	20
2.8 Ni-P-CNTs .....	20
2.9 Other NiP Composites Coatings .....	20
2.10 Ni coatings on 7075 Aluminum Alloy .....	21

Chapter 3.....	22
Experimental Method.....	22
3.1    Sample Preparation .....	22
3.2    Hypophosphite Treatment (Pre-Treatment) .....	23
3.3    Electroless Deposition – Coating Bath .....	24
3.4    Bath Composition: .....	24
3.5    The Nickel Source:.....	25
3.6    Reducing Agents:.....	25
3.7    Substrate.....	27
3.8    Analysis and Characterization Techniques .....	28
3.8.1    Scanning Electron Microscopy (SEM): .....	28
3.8.2    Energy Dispersive X-ray (EDX):.....	29
3.8.3    X-Ray Diffraction (XRD): .....	30
3.8.4    Atomic Force Microscope (AFM) .....	31
3.8.5    Microhardness – Vickers Hardness.....	32
3.8.6    Tafel Scan .....	33
3.8.7    Electrochemical Impedance Spectroscopy (EIS) .....	34
Chapter 4.....	37
Results and Discussion .....	37
4.1    XRD Analysis .....	37
4.2    SEM and EDS Analysis .....	39
4.3    AFM Analysis .....	44
4.4    Micro-hardness.....	46
4.5    Corrosion Analysis – EIS and Tafel Plots.....	49
Conclusions.....	55
References.....	56

## List of Figures

Figure 1. Chemical structure of dichromate on left and health hazards caused by hexavalent chromium Cr-VI and Cr-VI microbial reduction on right [10].....	3
Figure 2. Aluminum 7075 microstructure[11] and its products. ....	4
Figure 3. Pourbaix diagram of aluminum 7075 showing a relationship between potential and solution pH [12] .....	7
Figure 4. Phenomena of pitting corrosion for Al-7075 alloy.....	8
Figure 5. Electroless deposition setup for depositing coating[13].....	10
Figure 6. Image of scanning electron microscopy, its mechanism and types of different rays involved during electron interaction with the sample.....	29
Figure 7. X-Ray machine and X-ray interaction with the atomic lattice, its mechanism and phenomena of the Bragg's law[21]. ....	31
Figure 8. Mechanism behind the atomic force microscopy. The interaction of the cantilever tip with the sample surface. Resultant data is collected by photodiode, from which computer forms an image.....	32
Figure 9. The Vickers hardness tester and the indent measurement of the diamond shaped impression formed by the tip of the Vickers indenter.....	33
Figure 10. Potentiostat interface instrument through which the EIS and potentiodynamic polarization measurements can be measured. ....	35
Figure 11. XRD peaks for with and without pretreatment and with BN reinforced Ni-P composite coatings. ....	39
Figure 12. SEM images of (a) without pretreatment of the Al substrate, (b) with pretreatment, (c) Ni-P/BN (0.5g/L), (d) Ni-P/BN (1.0g/L), (e) Ni-P/BN (1.5g/L), and (f) Ni-P/BN (2.0g/L) composite coatings.....	40
Figure 13. SEM image of the cross-section of Ni-P coating, indicating the good adhesion of the coating with the substrate with Pre-Treatment and damaged / poor adhesion in without pretreatment .....	41

Figure 14. EDX in wt% of without pretreatment of the Al substrate, with pretreatment, Ni-P/BN (0.5g/L), Ni-P/BN (1.0g/L), Ni-P/BN (1.5g/L), and Ni-P/BN (2.0g/L) composite coatings. EDX graph is presented at the bottom ..... 42

Figure 15. Increase in the P content with deposition time (left), increase in the thickness of the coatings with increase in the deposition time (right) ..... 43

Figure 16. The relationship between P content in the deposits and their respective hardness values) ..... 44

Figure 17. AFM images of (a) without pretreated Al substrate, (b) with pretreatment, (c) Ni-P/BN (0.5g/L), (d) Ni-P/BN (1.0g/L), (e) Ni-P/BN (1.5g/L), and (f) Ni-P/BN (2.0g/L) composite coatings. .... 45

Figure 18. Nanoindentation graphs of (a) without pretreated Al substrate, (b) with pretreatment, (c) Ni-P/BN (0.5g/L), (d) Ni-P/BN (1.0g/L), (e) Ni-P/BN (1.5g/L), and (f) Ni-P/BN (2.0g/L) composite coatings ..... 48

Figure 19. Bode plots. (a) Phase angle vs log(f). (b) log |Zi| vs log(f) of without pretreated Al substrate, with pretreatment, Ni-P/BN (0.5g/L), Ni-P/BN (1.0g/L), Ni-P/BN (1.5g/L), and Ni-P/BN (2.0g/L) composite coatings..... 50

Figure 20. Circuit diagrams for EIS fitting of (a) without and with pretreated Ni-P coating and (b) without and with pretreated Ni-P/BN with different concentrations of BN reinforcements. .... 51

Figure 21. Nyquist plot of without pretreated Al substrate, with pretreatment, Ni-P/BN (0.5g/L), Ni-P/BN (1.0g/L), Ni-P/BN (1.5g/L), and Ni-P/BN (2.0g/L) composite coatings..... 52

Figure 22. Tafel plots of bare Al substrate, without pretreated Al substrate, with pretreatment, Ni-P/BN (0.5g/L), Ni-P/BN (1.0g/L), Ni-P/BN (1.5g/L), and Ni-P/BN (2.0g/L) composite coatings ..... 53

## List of Tables

Table 1. Chemicals and immersion parameters used for hypophosphite treatment .....	23
Table 2. Chemicals used for the electrolytic bath, its processing and optimized parameters.....	24
Table 3. Elemental composition of aluminum 7075 alloy .....	27
Table 4. Vickers hardness data and nanoindentation hardness data of without pretreatment, with pretreatment and Ni-P/BN composite coatings.....	47
Table 5. $I_{\text{corr}}$ and $E_{\text{corr}}$ data of without pretreatment, with pretreatment and Ni-P/BN composite coatings obtained from Tafel curves.....	54

## **List of Abbreviations**

EN	ElectrolessNickel
BN	Boron Nitride
FC	Friction Coefficient
CC	Chrome Coating
CCC	Chrome Conversion Coating
SEM	Scanning Electron Microscopy
EDS	Energy Dispersive Spectroscopy
SCC	Stress Corrosion Cracking
RRAT	Retrogression and Re-aging Treatment
GPa	Gigapascals
MPa	Megapascals
TWI	Taber Wear Index

XRD X-Ray Diffractometer

AFM Atomic Force Microscopy

# Chapter 1

## Introduction

Aluminum alloys have been used as a replacement of steel where ratio of strength and weight or an increased thermal / electrical conductivity are of the prime concern. It is evident from literature that aluminum alloys possess low hardness and inadequate tribological properties which limit their use in unprotected conditions such as harsh environments like CO<sub>2</sub>, H<sub>2</sub>S, Cl<sup>-</sup> and SO<sub>4</sub><sup>-2</sup> etc. Corrosion is another issue associated with aluminum alloys as oxide layer formed with higher porosity in corroding environment and this cause the localized corrosion reaction in selective areas. For the protection of aluminum alloys, one of the techniques is electroless deposition for the formation of protective layer over the aluminum alloys which results in enhanced mechanical and corrosion resistant properties[1].

This makes these structures practically useful in industries for instance in aircraft and aerospace to manufacture its different parts and components. Aluminum alloys are inexpensive, having low specific weight, excellent mechanical strength and better formability. The poor corrosion properties limit the widespread use of aluminum alloys in some environments where wear resistance high temperature and corrosion resistance is required. For this purpose, various anti-wear and anticorrosive strategies have been developed by researchers for the improvement of mechanical properties as well as electrochemical properties of aluminum alloys such as hardness, strength, resistance to wear, Coefficient of Friction (FC) and resistance against corrosive media or environment depending upon the application in use. With regard to this, researchers have used many elements in the protective coatings for protecting the aluminum alloy and these are chromium, nickel, titanium etc. among them, due to the better hardness, corrosion resistance and ductility, nickel is considered an imperative candidate to improve surface properties to resist reactions of the alloy with the environment.

To achieve desirable properties of aluminum alloys, various coating processes / techniques have been deployed like paints, electroless deposition, electrodeposition and anodization etc. Among them, electroless technique is a desirable technique because of the dense structures obtained with



less possible porosities and defects in the structure. Electroless Nickel-Phosphate plated coatings are mainly used as engineering coatings as they provide a perfect alternative to chrome coatings and also, they have much better hardness and resistance to wear / corrosion. These coatings also increase the materials performance while in service. [2]

## **1.1 Advance Surface Coating Techniques**

Presently Advanced Materials & Surface Engineering is gaining much attention therefore a range of methods are employed to enhance, repair, or modify the surfaces of base metals. Generally, modifications are being carried out via:

- Sputtering [3]
- Electron / Molecular Beam Epitaxy[4]
- Physical vapor deposition (PVD) [5]
- Chemical Vapor Deposition (CVD) [6]
- Spray Coating (low / high temperature)
- Plasma spray coatings [7]
- High-Velocity Oxy-Fuel (HVOF) [8]
- Sol Geletc.[9]

Additionally, deposition (electroless or electrodeposition both) are also significant methods in this domain.

## **1.2 Significance of the Project**

### **Chrome Coatings (CC) Hazards and Alternative to CC**

Chrome Conversion Coatings (CCC) have long been regarded as the ideal choice for protecting aluminum alloys against corrosion. However, in the past two decades, there has been growing concern about their toxicity and carcinogenic properties. The oral ingestion of chromates can lead to various health problems, including changes in blood composition, liver and kidney failure, damage to the gastrointestinal system, lung cancer, and intestinal tumors. In addition to these issues, skin damage has been observed, and inhaling chromates can also lead to lung cancer.

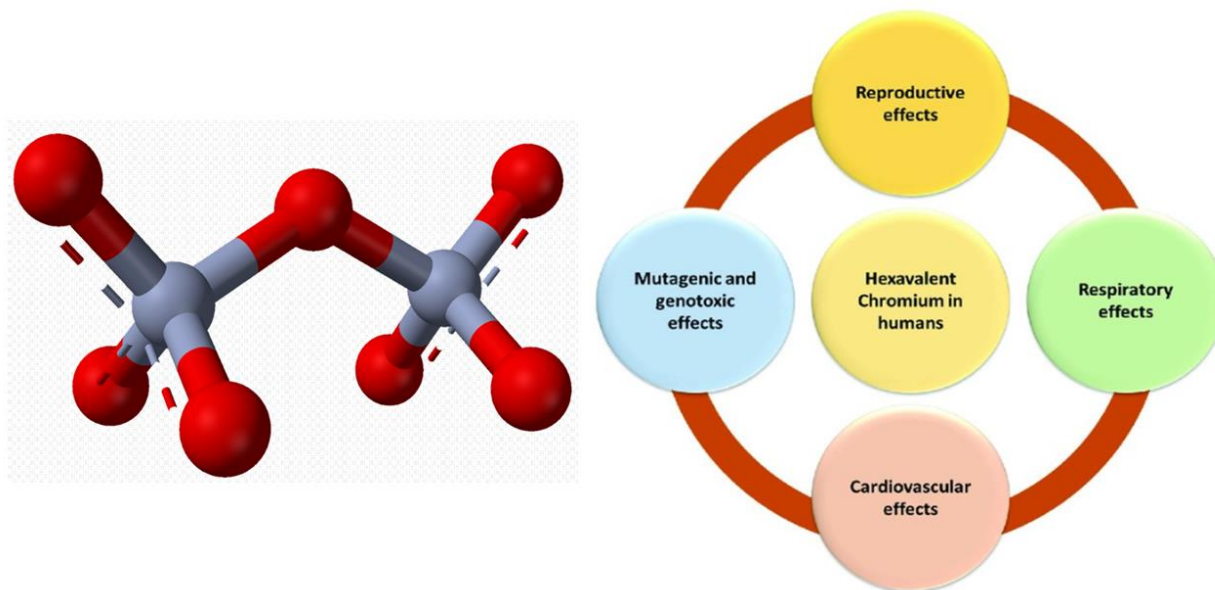


*Figure 1. Chemical structure of dichromate on left and health hazards caused by hexavalent chromium Cr-VI and Cr-VI microbial reduction on right [10].*

Hexavalent Chrome (Cr (VI)) has been a preferred choice for many industries due to its effectiveness in reducing corrosion and enhancing corrosion resistance. However, research suggests that Cr (VI) can react within human cells in the presence of reducing agents, producing chrome with lower valencies ( $3^+$ ,  $4^+$ , or  $5^+$ ), along with oxygen, leading to changes in DNA. Given these concerns, there is a pressing need to develop alternative corrosion-resistant coatings that do not rely on Chromium (VI). Efforts are currently focused on creating environmentally friendly anticorrosive coatings. While there are different coating systems with the potential to replace chrome conversion coatings, they have not yet fully met the benchmark standards in terms of processing and anticorrosive properties. The use of chromates has been restricted due to their environmental impact, with the permissible exposure limit for Chrome (specifically  $\text{Cr}^{6+}$ ) reduced from  $52\text{mg}/\text{m}^3$  to  $5\text{mg}/\text{m}^3$  since 2008 by the Occupational Safety and Health Administration (OSHA). Consequently, there is an urgent need to explore alternatives to CCC for protecting aluminum alloys.

### 1.3 Al-7075 -T6 Substrate

Aluminum Alloy 7075-T6 is widely utilized in applications that demand a combination of high strength and reduced weight. However, its utility in high-end applications is constrained by the occurrence of localized corrosion, as well as its susceptibility to adhesion and relatively lower hardness, which collectively result in suboptimal tribological properties. The formation of galvanic coupling in these alloys is contingent upon the distribution of intermetallics and strengthening particles. This galvanic coupling primarily leads to corrosion initiation which further change to pitting or intergranular exfoliation corrosion. Micro-capillary studies have revealed that the matrix in Al-7075-T6 alloy exhibits greater electrochemical activity than the intermetallics, specifically  $Al_7Cu_2Fe$  and  $(Al,Cu)_6(Fe,Cu)$ . Notably,  $MgZn_2$  particles, which are found in nanometer-sized ranges, serve as the primary strengthening agents. During heat treatment, these particles precipitate along grain boundaries, contributing to intergranular corrosion due to their heightened reactivity compared to the matrix [11].

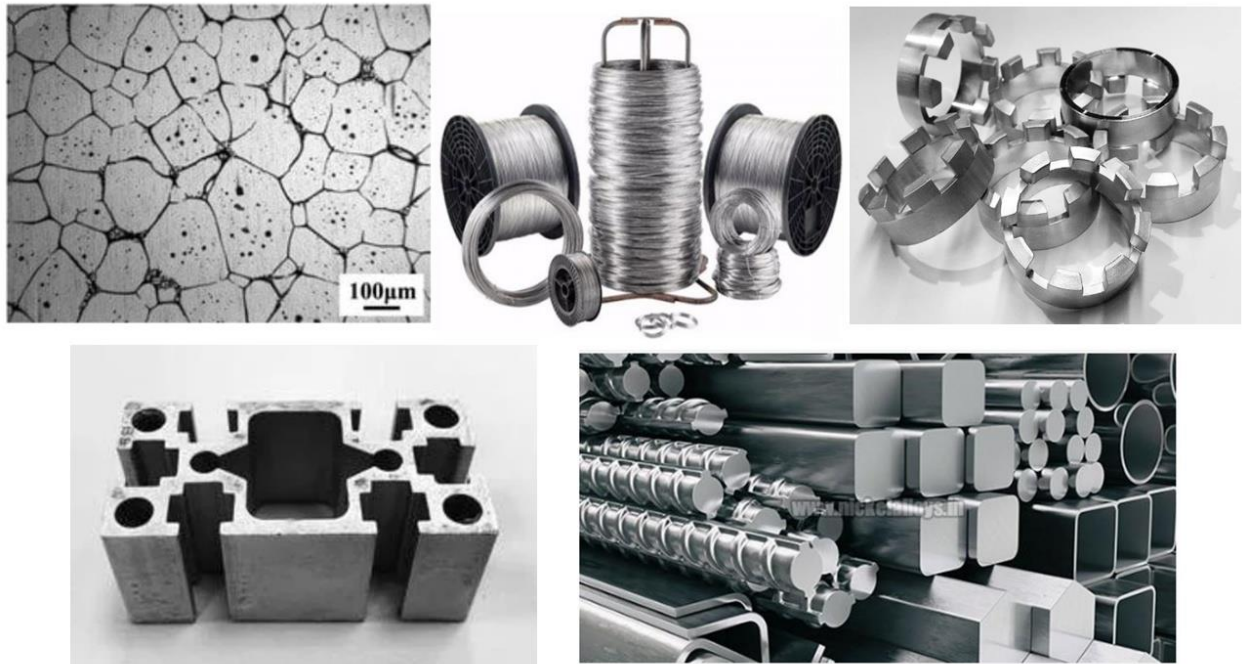


*Figure 2. Aluminum 7075 microstructure[12] and its products.*

## 1.4 Corrosion in Al-7075

Aluminum Alloys, particularly those belonging to the 7xxx series, are favored in the production of aircraft structures due to their excellent combination of mechanical properties, including strength, toughness, fatigue resistance, and low density. However, despite these advantageous characteristics, these alloys are susceptible to localized corrosion in various forms, namely intergranular, stress cracking, and exfoliation corrosion. One common approach to enhance their properties is through heat treatment, with the T6 process being employed to achieve high strength. Unfortunately, this treatment does not significantly improve the alloys' resistance to localized corrosion. To address this issue, over-aging treatments like T73, T76, and T74 are utilized, albeit at the expense of some strength. Research has also indicated that the Retrogression and Re-aging Treatment (RRA) can provide a modest increase in stress corrosion cracking (SCC) resistance without compromising the alloy's strength. Furthermore, it has become clear that corrosion resistance can be enhanced by employing suitable heat treatments, such as High Temperature Pre-Precipitation, or by applying passive or protective coatings to shield the alloy from environmental factors, thereby prolonging its lifespan[13].

Preserving aluminum alloys from corrosion has garnered significant interest and stands as a prominent topic in the field of electrochemistry. Over an extended period, there has been a strong tendency towards protecting aluminum alloys through the application of durable protective coatings designed to offer an extended lifespan, typically ranging from 20 to 30 years. Aluminum Alloy 7075, renowned for its use in military and aerospace applications, has remained a central focus of these efforts. The composition of Al-7075 alloy primarily consists of three major alloying elements: Zinc, Copper, and Magnesium. These elements are responsible for the alloy's specific composition. The intermetallic compounds resulting from the combination of Zinc and Copper exhibit cathodic properties in relation to the matrix, which is Aluminum in this instance. Conversely, the intermetallics formed with Magnesium display anodic characteristics[14].

Numerous research studies have established that the primary form of corrosion in Al 7075 alloy is localized corrosion, encompassing pitting, exfoliation, and intergranular corrosion, among others. This type of corrosion is intricately linked, either directly or indirectly, with the presence and distribution of the aforementioned intermetallic compounds. These intermetallics exhibit different reactivity concerning the matrix, which is Aluminum. Some are cathodic, while others are anodic,

creating a galvanic coupling effect. The key intermetallic compounds identified in Al-7075 Alloy include  $\text{Al}_7\text{Cu}_2\text{Fe}$  and  $(\text{Al,Cu})_6(\text{Fe, Cu})$ , which are relatively less active and, as a result, tend to dissolve in the surrounding environment. In contrast,  $\text{MgZn}_2$ , which precipitates along grain boundaries during heat treatments, is more reactive. This disparity in reactivity is responsible for the occurrence of intergranular corrosion in Al-7075 T6 alloy[11].

## 1.5 Corrosion Protection of Al-7075

Several factors contribute to the corrosion of Al-7075 alloy when its surface comes into contact with moisture:

- **Oxidation:** which involves an anodic reaction.
- **Reduction:** leading to a cathodic reaction.
- **The transfer of charged particles:** such as ions and electrons, through any electrolyte.

Al-7075 alloy demonstrates good resistance to various environmental conditions and the reason is the formation of an oxide layer, specifically  $\text{Al}_2\text{O}_3$ , that serves as a protective shield to the underlying alloy. However, it's important to note that this oxide layer is less stable in acidic or basic environments, where it either inhibits its formation or weakens its protective properties.

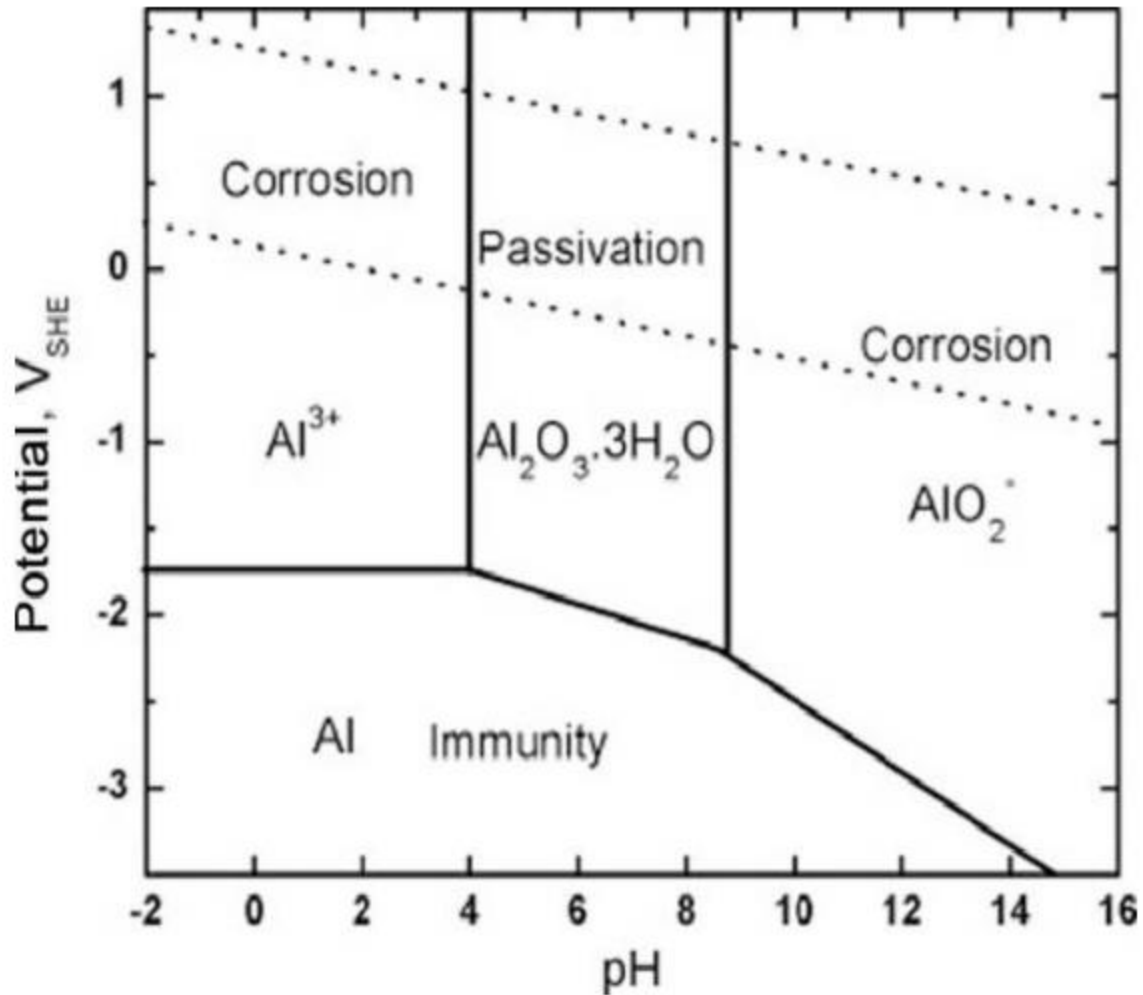
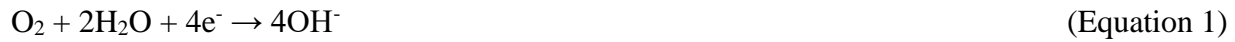


Figure 3. Pourbaix diagram of aluminum 7075 showing a relationship between potential and solution pH [15]

Copper and copper-based intermetallic compounds play a crucial role in the corrosion of aluminum alloys. Alloys without copper tend to be more resistant to corrosion compared to those containing copper. Pitting corrosion, in particular, is influenced by a concept called pitting potential, which represents a potential level above which pit formation occurs, and below which the material remains pit-free. The presence of chloride ions (Cl<sup>-</sup>) promotes pit formation by breaking down the protective Al<sub>2</sub>O<sub>3</sub> layer, forming AlCl<sub>3</sub>.

The process of pitting corrosion involves two stages: initiation and growth. Initiation is associated with the potential difference between the intermetallic compounds and the surrounding matrix, which is primarily aluminum in the case of Al-7075 T6. In this alloy, smaller pits tend to merge,

forming larger pits, especially when exposed to a sodium chloride solution. The outer sides of the pit become cathodic, reducing oxygen by reacting with water as follows:



This reaction is responsible for preventing metal dissolution in the areas outside the pit because a large cathode-to-anode ratio promotes the anodic reaction. However, the regions inside the pit remain active, and the following reaction takes place:



An electrical imbalance within the pit leads to the formation of HCl which occurs due to incremental change of negative ( $\text{Cl}^-$ ) ions, which reduces the pH:

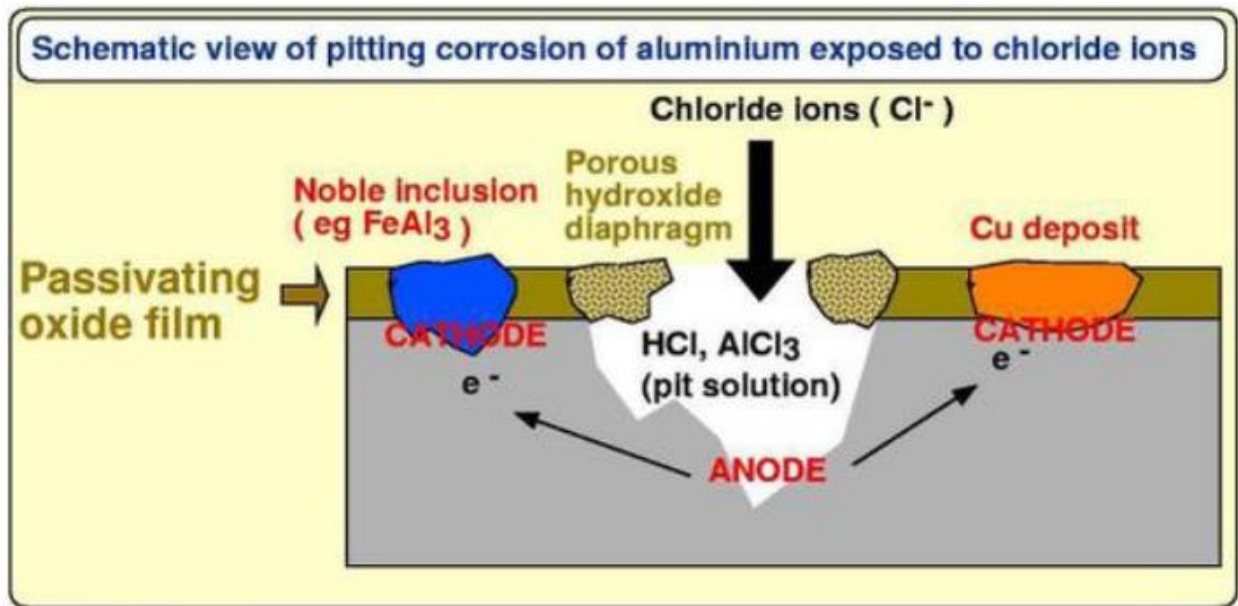


Figure 4. Phenomena of pitting corrosion for Al-7075 alloy [14]

Crevice corrosion in aluminum alloys is a problem that occurs when there's a gap between two surfaces, with one of them being metal, and the liquid in the gap is still or stagnant. Just like discussed with equations (1) and (2), both anodic and cathodic reactions happen on the metal surface, but inside the crevice, things are a bit different. In there, it's hard for oxygen to replace

itself, which means that the anodic reaction, which is the one that corrodes the metal, gets a boost inside the crevice. Meanwhile, outside the crevice, the cathodic reaction, which is the one that helps protect the metal, takes place more.

Because of this difference in how these reactions happen, we see an increase in chloride or hydrogen ions within the crevice. This leads to a lower pH level, which, in turn, makes corrosion worse inside the crevice[16][17].

Given how crucial Al-7075 alloy is in the aerospace and automobile industries, there's a strong focus on protecting it from corrosion. One effective method for this is creating a layer which protects the alloy. An example of such a solution is using a nickel phosphorus coating to enhance the alloy's resistance to corrosion[14].

Al-7075 alloy is particularly susceptible to corrosion when exposed to chloride ions. This can be a challenge, especially in marine environments or when the alloy comes into contact with water that has dissolved chloride ions. Additionally, the natural oxide layer on aluminum alloys is quite thin, making long-term protection difficult without further treatments. One approach to addressing this is to thicken the  $\text{Al}_2\text{O}_3$  layer artificially through chemical or electrochemical methods.

There are three main ways to reduce corrosion in aluminum alloys:

- **Barrier Protection:** This method involves using organic or inorganic coatings to shield the alloy from the environment. These coatings not only provide a physical barrier but also limit the transfer of charged particles.
- **Active Corrosion Protection:** In this strategy, the corrosion cell processes are slowed down by introducing inhibitors that reduce the permeability of chloride ions. These inhibitors act to hinder the corrosion process.
- **Conversion Coatings:** This approach involves removing the native oxide layer and forming a new oxide layer, which serves as a protective barrier. Chromate-based conversion coatings are commonly used due to their cost-effectiveness and efficiency. In these coatings, the transition of chromium ions from  $\text{Cr}^{6+}$  to  $\text{Cr}^{3+}$  plays a significant role in corrosion resistance.  $\text{Cr}^{6+}$  ions also contribute to the self-healing properties of the coating when it's damaged by corrosive attacks. These chromate coatings chemically form protective layer on the surface on metal which act as a barrier against corrosion[18].



## 1.6 Different Techniques of Electrochemical Deposition

In the realm of electrochemical deposition, you'll find a variety of techniques. These include electroless deposition, electroforming, and different approaches to electrodeposition, like direct current, pulse current, pulse reversed current, and the utilization of lasers to enhance the deposition process.

### 1.6.1 Electroless Deposition

Deposition via electroless route is a unique technique / process that involves the autocatalytic reduction metallic ions, resulting in the creation of a thin film or coating. This reduction occurs through the oxidation of specific chemical in the solution, known as reducing agents. During this process, the reduction of metallic cations occurs by acquiring electrons, which can come from either the substrate itself or a catalyst. This fascinating self-catalyzing reduction process that leads to the formation of a metallic coating on a substrate is commonly referred to as electroless plating.

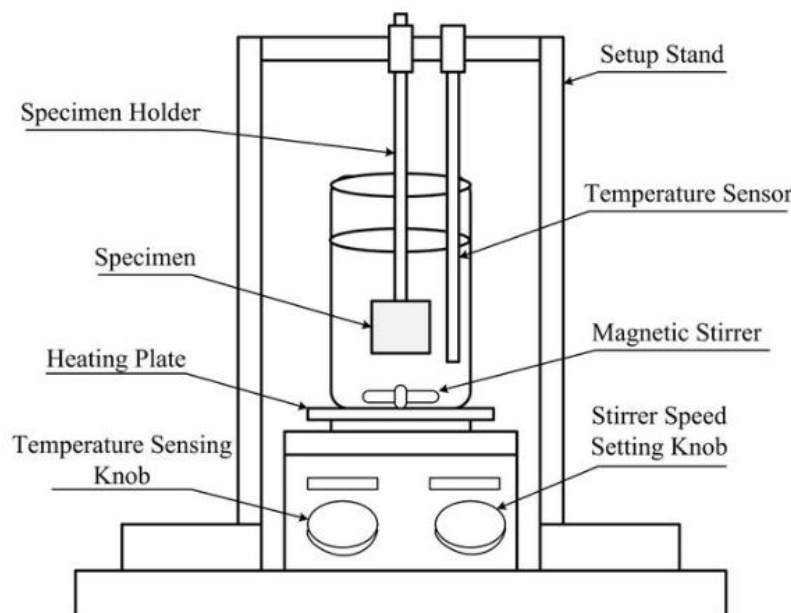


Figure 5. Electroless deposition setup for depositing coating[19]

It's worth noting that certain processes, like immersion plating and silvering, which deposit materials without the use of an electric current, are not considered part of electroless plating. In immersion or galvanic plating, the substrate's material dissolves, and the solution provides metallic ions that got reduced on the surface of the metallic material. Notably, in these processes, there isn't

a specific reducing agent; instead, the base metal/substrate itself acts as a reducing agent. However, the drawback of such methods is that they often result in coatings with poor adhesion.

On the contrary, electroless deposition, or coating, offers significant advantages, particularly in terms of improved corrosion resistance and enhanced wear resistance. Within the realm of electroless-deposition, electroless nickel deposition has gained considerable commercial importance. There are several types of electroless Ni coatings, including pure nickel, electroless nickel binary alloy (NiP) coatings, and electroless nickel composite coatings (NiPX) where X could be any ceramic micro or nano particles. These coatings have diverse applications across various industries.

### **1.6.2 Factors Affecting Electroless Bath**

Several factors are of vital importance in influencing the process of metal deposition or electroless deposition. These factors encompass pH level, bath temperature, composition, agitation speed, the presence of additional agents, potential impurities in the electrolyte, state of the substrate surface i.e. physical and chemical both, and the specific anions and cations within the electrolyte solution.

### **1.6.3 Advantages of Electroless Deposition**

- Quality of Deposit
- Better physical / mechanical properties
- Uniformity (bind holes to sharp corners)
- Properties variation via varying pH, Temperature and Composition of bath

Generally, an electroless bath contains following:

- Metal Ions (Source of Metal)
- Reducing Agent (provide electron which used to reduce metal)
- Complexants (Control free metal ion concentration)
- Accelerate (Speed up reduction and deposition)
- Stabilizer (control deposition by shielding catalytically active deposition)
- Buffer (pH adjustment)

- Temperature (provides energy for depositing the metal)

The growing interest in electroless plating has been fueled by advancements in scientific fields such as surface sciences, as well as in purification and separation techniques. Interestingly, the practice of depositing metallic nickel through electroless deposition using hypophosphate dates back to 1844. In the 1950s, the American automobile industry played a significant role in the development of electroless plating by reduction, a technique that gradually replaced traditional electroplating methods.

## 1.7 Electroless Deposition of Nickel Phosphate

### Detailed process

In electroless deposition of any metal, salts of that metal are used which involve electrochemical reactions like oxidation and reduction. In other words, transference of electrically charged species take place. Basic difference between two processes is listed below:

#### Oxidation

- Loss of Electron
- Anodic Process

#### Reduction

- Gain of Electron
- Cathodic Process

For simplicity, it can be considered that metal displacement reactions are also electroplating reactions.

One of the simplest and fascinating processes in chemical plating is known as the metal displacement reaction. Imagine immersing zinc metal in a solution which is copper sulfate solution; what happens is a captivating chemical transformation. In this process, the less noble zinc atoms on the metal's surface dissolve, and they are replaced, almost magically, by copper atoms from the solution. We can describe this phenomenon through two key reactions:

**Oxidation:** Zinc (Zn) loses electrons and turns into  $Zn^{2+}$  ions, releasing two electrons (anodic, with a standard electrode potential  $E_0$  of 0.76 V).

**Reduction:** Copper ions ( $\text{Cu}^{2+}$ ) gain these two electrons, reducing to form solid copper (Cu) (cathodic, with a standard electrode potential  $E_0$  of 0.34 V).

The overall result is that the zinc (Zn) combines with copper ions ( $\text{Cu}^{2+}$ ) to create zinc ions ( $\text{Zn}^{2+}$ ) and solid copper (Cu) (with an overall electrode potential  $E_0$  of 1.1 V).

This process continues until a significant portion of the zinc substrate is deposited with copper. When this happens, the zinc dissolves and the deposition of copper nearly come to a halt. However, the deposits formed through chemical plating by displacement are relatively thin, typically ranging from 1 to 3 microns. This limitation makes this method less commonly employed for substantial plating applications.

To create thicker deposits using a chemical approach without consuming the substrate, a different strategy is necessary. Here, the oxidation reaction should ideally be used without dissolving the substrate. The initiation of the deposition process should must be carried out only on the substrate surface so that initial deposit could be build up. This chemical process has more positive redox potential as compared to the metal deposition via immersing.

The deposition of nickel metal using hypophosphite is one such method that meets the oxidation and redox potential criteria while preserving the substrate's mass. The reaction involves both reduction and oxidation equations, resulting in nickel deposition accompanied by the evolution of hydrogen.

Brenner and Riddell were the first one who introduced the terminology of electroless plating and they did it via explaining a process in which metal was plated on a substrate and there was no need of external source of energy or more precisely current. With passing time, electroless plating or deposition was changed in to a process of depositing a metal from an aqueous solution where selective reduction of metallic ions take place. This all occur on the surface of the metallic immersed in the solution. This process also involve certain catalytic activation of the substrate surface.

The term "electroless plating" firstly introduced by Brenner and Riddell is used to tell a method of how to plate metallic substrates with nickel or cobalt alloys, all without the need for an external DC source of electric current. Over time, the term "electroless plating" has broadened to include

any method that consistently deposits metal from a liquid medium. In summary, electroless plating involves the specific reduction of metal ions, taking place exclusively at the surface of a catalytic substrate immersed in a solution containing these ions. The presence of the current deposit catalyzes and sustains the deposition process on the substrate.

Since the deposit catalyzes the reduction reaction, the term "autocatalytic" is used to describe this plating process. In 1844, Wurtz observed that hypophosphite anions can reduce nickel cations. However, his experiments merely produced a black powder. It wasn't until 1911 when Breteau was the one who achieved metallic deposits of nickel-phosphorus alloys which were fully bright. In 1916, Roux was presented the first patent for an EN plating bath, although these early baths had a tendency to decompose spontaneously and form deposits on any surface they came into contact with, even the walls of the container.

Over the years, researchers continued to study this process, though their primary interest was in the chemical reaction rather than the plating process itself. In 1946, Brenner and Riddell published a significant paper, outlining the conditions for achieving proper electroless deposition as defined earlier. Since then, the electroless plating process has undergone further investigations and expansion by many researchers, leading to its current state of development.

EN plating has become an immensely vital catalytic plating process being employed today. Its extensive commercial and industrial utilization is attributed to the exceptional properties of EN deposits. These properties can vary based on the composition of the EN coating, which, in turn, is influenced by the operating and formulation conditions of the EN deposition bath. Naturally, an EN solution contains components such as a source of Ni ions, complexing agents, a reducing agent, energy and stabilizers/inhibitors. This procedure has evolved over time and has become a highly valuable and widely applied technique in various industries.

The most preferred source of Ni cations in the electroless plating process is Ni sulfate. Although other Ni based salts like nickel acetate and nickel chloride are occasionally used for specific applications, they have limitations. For instance, the chloride anion in Ni chloride can cause issues when EN plating is used on aluminum or as a shielding coating over iron-based alloys in corrosion-resistant applications. The use of Ni acetate, while possible, doesn't significantly enhance bath

performance or the quality of the deposit when compared to nickel sulfate. Any marginal advantages offered by nickel acetate are negated by its higher cost compared to nickel sulfate.

An ideal source of nickel ions would be the nickel salt of hypo-phosphorous acid,  $\text{Ni}(\text{H}_2\text{PO}_2)_2$ . Using nickel hypophosphite has the advantage of eliminating the need for sulfate anions and minimizing the accumulation of alkali metal ions. Additionally, it helps replenish the reactants consumed during the metal deposition process. The concentration of Ni ions and its interplay with the complexing and reducing agents will be explored further in an upcoming chapter.

## **1.8 Aims and Objectives**

The aims and objectives of this work is to obtain the homogeneous, crackles and well adhered Ni-P and Ni-P/BN composite coating on Al7075 substrate via electroless deposition technique. The adherence of the coatings with the Al7075 substrate has been one of the main concerns of the researchers for years. In this work, the substrates without pretreatment, with pretreatment and with composite coatings of Ni-P/BN were made, optimized and compared. The adhesion of the coatings was made better with substrate. Different concentrations of BN i.e. (0.5, 1.0, 1.5 and 2.0) g/L were added in the coatings and their mechanical and corrosion resistant properties were studied.

## **1.9 Overall Dissertation Outline**

This dissertation consists of five chapters whereas 1<sup>st</sup> chapter discusses the introduction containing motivations and background. In the 2<sup>nd</sup> chapter, the extensive review is taken place regarding our work in which Ni-P coatings and their properties are listed as observed by the researchers up till now. The 3<sup>rd</sup> chapter insights the work methodologies and experimental procedure during the whole research and extensively explained. It also contained the characterizations techniques and parameters used for each characterization. 4<sup>th</sup> chapter discusses all the results obtained, their analysis and elaborately discussed. In this chapter the coatings without pretreatment of the substrate, with pretreatment of the substrate and coatings with various concentration of BN nanoparticles i.e. (0.5, 1.0, 1.5, 2.0) g/L are discussed and their comparison is made. 5<sup>th</sup> chapter covers the conclusion of the work. 6<sup>th</sup> chapter contained the references that were utilize to get the clear insight and understanding towards the thesis writeup.

## **Chapter 2**

### **Literature Review**

In this chapter, we will provide a concise overview of the existing literature related to the research topic, which is focused on investigating the impact Development of Corrosion Protection Coating

System for Aerospace Grade Aluminum 7075 Alloy. We will explore various binary and ternary alloy coatings that incorporate different types of inclusions, and we will discuss the findings and insights shared by researchers in this field.

## 2.1 Ni-P Coatings

Moo Hong Seo et al [20] conducted a study examining the influence of ( $\text{H}_3\text{PO}_3$ ) acid concentration on the electrochemical deposition of Ni-P coatings. They utilized alloy 600 plates as substrates and looked into the phosphorous content in deposits obtained from both sulfamate and sulfate baths. Their research indicated that deposits from the sulfate bath incorporated phosphorous more effectively than those from the sulfamate bath. Furthermore, their investigation of current efficiency revealed that higher concentrations of  $\text{H}_3\text{PO}_3$  led to decreased current efficiencies in both types of baths.

The study also delved into the stresses produced within the deposits. The findings showed that stress levels in the deposits increased linearly with higher concentrations of  $\text{H}_3\text{PO}_3$  in both sulfamate and sulfate baths. The stress values increased from 45.9 to 74.8 MPa for sulfamate baths and from 106 to 144.8 MPa for sulfate baths. The deposits were examined using optical microscopy, which revealed a laminar structure. Transmission electron microscopy (TEM) was used to determine the microstructure, revealing a cell structure with grains densely surrounded by dislocations. After heat treatment effect,  $\text{Ni}_3\text{P}$  precipitates were predominantly found at the grain boundaries, with their shape transforming from round to needle-like between temperatures of 343 to 490°C. Thermal analysis demonstrated two exothermic peaks, one attributed to  $\text{Ni}_3\text{P}$  ppt and the other to recrystallization at 575°C.

D.H. Jeon et al [21] investigated the hardness and its relationship with the wear resistance of Ni-P nanocrystalline deposits. They employed low carbon mild steel (AISI 1010) as the substrate with a bath temperature of 70°C and pH 1.5. X-ray diffraction (XRD) results indicated line broadening in the diffraction pattern, signifying a decrease in grain size with increased P content. The average grain size measured by XRD was close to 1 nm. The study found a connection between the hardness of the coatings and phosphorous content, with Taber wear index (TWI) inversely proportional to hardness. It was observed that in nano-crystalline Ni-P coatings, hardness and



abrasive wear resistance had a linear relationship. Heat treatment resulted in increased hardness due to Ni<sub>3</sub>P precipitation, leading to a decrease in TWI.

Tsutomu Morikawa et al [22] employed a Ni citrate electrolyte for depositing Ni-P alloy coatings through electrodeposition. They used Cu sheets as substrates and investigated the effects of H<sub>2</sub>PHO<sub>3</sub> concentration, bath pH, current density, and temperature. The study revealed that the current efficiency reached a highest value with a concentration of 0.2M H<sub>2</sub>PHO<sub>3</sub>. As the current density increased up to 10A/dm<sup>2</sup>, the current efficiencies for both Ni and P decreased. Higher bath temperatures increased the current efficiencies for both Ni and P in the deposition of Ni-P, and a similar trend was observed with increased bath pH. These findings indicated a strong interaction between Ni and Ni-P during Ni-P alloy deposition, suggesting the formation of the alloy through a direct deposition mechanism. Additionally, the study observed the formation of PH<sub>3</sub>, Ni<sub>2</sub>P, Ni<sub>3</sub>P and at low bath pH.

## **2.2 Ni-P-Si<sub>3</sub>N<sub>4</sub> Coatings**

J. N. Balaraju et al [23] made electroless Ni-P-Si<sub>3</sub>N<sub>4</sub> high phosphorous coatings. Composite coatings were produced by adding submicron silicon nitride particles to a hypophosphite-reduced electroless nickel bath, resulting in coatings with enhanced hardness. Analysis showed consistent phosphorus content in both pure Ni-P and composite coatings. The structure and phase change behavior remained unchanged due to particle incorporation. An increase in nodular size was observed after annealing at the crystallization temperature. The composite coatings exhibited 10% improved hardness in the as-received state with inclusion of 1g/L and a 22% increase after annealing, primarily attributed to the Si<sub>3</sub>N<sub>4</sub> particles.

J.N. Balaraju et al [24] studied electroless Ni-P-Si<sub>3</sub>N<sub>4</sub> composite coatings using a low-phosphorus content in the electrolytic bath with submicron-sized Si<sub>3</sub>N<sub>4</sub> particles, and plain Ni-P coatings were prepared and compared. The phosphorus content in the electroless pure Ni-P alloy and Ni-P-Si<sub>3</sub>N<sub>4</sub> coatings was found to be 3.7% and 3.4%, respectively. SEM images exposed that the Si<sub>3</sub>N<sub>4</sub> particles were homogeneously distributed all over the thickness of the composite coatings, increasing the nodularity compared to plain Ni-P deposits. Electrochemical studies in a sodium chloride solution indicated a slight reduction in corrosion current density and a greater polarization resistance for the low-phosphorus composite coatings compared to plain Ni-P deposits. Electrochemical

impedance studies revealed two-time constants behavior, potentially due to the cauliflower morphology, with higher charge transfer resistance ( $R_{ct}$ ) values indicating improved corrosion resistance in the composite coatings, findings which were corroborated by SEM analysis of corroded samples.

### **2.3 Ni-P- $Al_2O_3$**

Alumina particles increase the tribological properties of the NiP coating including its mechanical properties. There is a direct relationship between concentration of the  $Al_2O_3$  and the hardness of the coating which is further augmented by heat treatment at 400°C. There is a phase transition observed at temperature 350°C to 400°C from amorphous to crystalline and as a result improve all the related properties like hardness, corrosion resistance, morphology etc. At heat treatment above 400°C, a coarse  $Ni_3P$  phase is formed which is responsible for the reduction of hardness[25].

### **2.4 Ni-P-SiC**

Silicon Carbide is one of the most considered reinforcement as it increases the strength of the coating along with its erosion / corrosion resistance. Similar to addition of  $SiO_2$  in NiP, SiC also increase the hardness and at 400°C maximum hardness increase observed due to phase change i.e. semi-coherent to non-coherent  $Ni_3P$  after 400°C. As compared to nano-SiC, addition of micro particles of SiC provides better properties on steel. At 2g/L concentration, a better corrosion resistance observed for steel. On Copper and AZ 31 magnesium alloy, 1g/L SiC (nanoparticles) showed better corrosion resistance and 4g/L concentration of SiC particles enhanced corrosion resistance of AZ91D Mn Alloy. In comparison to  $TiO_2$  and  $ZrO_2$ , SiC based NiP shows better corrosion resistance. For Aluminum Alloy, SiC increased the wear resistance along with the corrosion resistance.

### **2.5 Ni-P- $SiO_2$**

With an increase of phosphorus content in NiP coatings, the surface roughness of the coating also increased and in this regard addition of  $SiO_2$  (nanoparticles) reduced the surface roughness. In case of NiP with a medium P content, an amount of 2g/L  $SiO_2$  reduced the porosity of the coating via

forming a nodular structure. Medium P content in NiP with SiO<sub>2</sub> showed better corrosion resistance and when such coatings heat treated at 400°C microhardness increase 3 to 4 times over a steel substrate. Above 400°C, the hardness starts to decrease and as a result wear resistance also get reduced.

## **2.6 Ni-P-ZnO**

ZnO based NiP coating improved the microhardness by 60% on mild steel and an overall improvement of corrosion resistance was also observed.

## **2.7 Ni-P-TiN**

Electroless deposition of NiP coating with TiN showed better corrosion resistance as compared to the one with Alumina, Silicone Carbide, Silica or Zinc Oxide. Heat Treatment of coating at a temperature of 400°C, increased the micro hardness by 90%.

## **2.8 Ni-P-CNTs**

Carbon Nanotubes grabbed the attention of researchers due to their structure and extra ordinary properties related to load transfer resistance or electrochemical. Hardness of NiP coating increase with an addition of CNTs up to 1.1% g/L and further addition reduce it. On Aluminum Alloy (Al-5083), NiP-CNTs with a high phosphorus content led to a better or improved corrosion resistance.

## **2.9 Other NiP Composites Coatings**

Nickel Phosphorus (NiP) with Titanium Dioxide or Alumina (Al<sub>2</sub>O<sub>3</sub>) showed an increase in hardness and corrosive resistance on Copper Substrate. On copper substrate, hardness of Alumina based NiP was more than that of TiO<sub>2</sub> based.

- On Nickel Foil, TiO<sub>2</sub> solution (rather than particle based) increase corrosion resistance along with micro-hardness.
- Corrosion resistance of NiPW is more than NiP with Alumina on a low carbon steel substrate
- NiP deposited via electroless deposition impart better corrosion / wear resistance but at the same time offer high friction coefficient and for this PTFE can be used to reduce friction coefficient.

- Heat Treatment of NiP on martensite steel enhanced the wear resistance and this due to the presence of hard crystalline phase of Ni<sub>3</sub>P.
- Ni-Ti particles in NiP also increase the corrosion resistance.

S.Ranganatha et al [26] fabricated Ni-P-HNT composite coatings for high performance applications. HNTs are a type of naturally occurring aluminosilicate clay characterized by their predominantly hollow nanotube structure, sourced from natural environments. Composed mainly of a two-layered aluminosilicate with the chemical composition  $\text{Al}_2\text{Si}_2\text{O}_5(\text{OH})_4 \cdot 2\text{H}_2\text{O}$ , they bear resemblance to minerals like kaolinite, dickite, and nacrite, primarily differing in crystal morphology. HNTs represent a layered clay mineral, with one silica tetrahedron sheet and one alumina octahedron sheet in a 1:1 stoichiometric ratio. The length of HNTs can vary within the range of 1 to 15 micrometers. These nanotubes possess an internal diameter of 10–30 nanometers and an external diameter of 50–70 nm, contingent on the specific deposits. The outermost surface of HNTs exhibits chemical properties akin to  $\text{SiO}_2$ , while the inner core is associated with the properties of  $\text{Al}_2\text{O}_3$ . Hollow nanotubes have garnered substantial interest in scientific and industrial circles due to their unique physical and chemical attributes stemming from their structural versatility. They offer promising prospects for advanced applications in diverse fields, including catalysis, electronics, energy storage, optics, and biological systems.

## **2.10 Ni coatings on 7075 Aluminum Alloy**

Mohan Kumar et al [27] fabricated Ni coatings on aluminum alloy 7075 to study fracture toughness and mechanical properties of the substrate. The thickness of the deposits came out to be 10-20  $\mu\text{m}$ . The study on the fracture and mechanical properties of the Al 7075-T6 coated alloy revealed an interesting finding. There is a clear and consistent correlation between the hardness, yield strength and ultimate tensile strength values. Notably, as the thickness of the electroless nickel (EN) coating increases, the tensile and fracture toughness properties of the Al 7075-T6 alloy also improve. This improvement is attributed to a significant change in the nature of crack propagation. The uncoated aluminum alloy exhibits a critical load (PQ) carrying capacity of 4.4 kN, corresponding to a K<sub>Ic</sub> value of 22.8  $\text{MPa}\sqrt{\text{m}}$ . In contrast, the aluminum alloy coated with 10  $\mu\text{m}$  and 20  $\mu\text{m}$  of electroless nickel (EN) coating shows higher critical loads of 6.67 kN and 7.41 kN, with corresponding K<sub>Ic</sub> values of 34.48  $\text{MPa}\sqrt{\text{m}}$  and 37.67  $\text{MPa}\sqrt{\text{m}}$ , respectively. The presence of the EN coating results

in a shift from unstable crack growth to a more stable crack growth pattern due to the robust bonding between the electroless nickel coating and the aluminum alloy. Additionally, hardness values can serve as a reliable indicator for the tensile strength of alloy. Examination of the cracked surface of the EN-coated specimen using scanning electron microscopy revealed a more controlled and stable crack growth compared to the bare alloy.

## **Chapter 3**

### **Experimental Method**

This chapter provides a detailed account of the procedures involved in preparing the substrates and samples, putting light on the methodology that guided the entire research project. It also introduces the characterization techniques employed to analyze the samples.

#### **3.1 Sample Preparation**

Aluminum 7075-T6 was taken as a substrate sheet which was cut in the dimension of (50 x 50 x 2) mm<sup>3</sup>. After that, all the samples were mechanically grinded using silicon carbide (SiC) paper up to 2400 grit size starting from 400 in a sequence. Then they were polished with Alumina Paste with 50µm alumina particle size. After grinding and polishing, the Al substrate was cleaned with

Distilled Water and washed in ultrasonic bath which contains Acetone, for 5 min at Room Temperature. This was done to remove any rust or impurities that might come during polishing. Al substrates were etched in basic solution of 10% NaOH for 2 min at 70°C. In Sodium Hydroxide solution, reaction takes place which create a textured and roughened surface which is due to the development of soluble aluminum hydroxide ions  $Al(OH)_4^-$ . Moreover, it was observed that dissolution of Aluminum in NaOH solution forms Hydrogen Gas Bubbles and sample turned black. This is justified with the fact that Aluminum is an alloy that dissolved in acid and base both therefore it dissolved in NaOH solution leaving Cu layer behind which does not dissolve in basic solution. After the alkaline etching, samples were dipped in 50% solution of  $HNO_3$  which removed the black layer on the sample formed while alkaline. As already mentioned, alkaline etching leave Copper and  $HNO_3$  dissolve that layer to activate it. Dipping in 50%  $HNO_3$  was also done to activate the surface of the aluminum substrate.

### 3.2 Hypophosphite Treatment (Pre-Treatment)

The following step includes treating the aluminum surface with a solution that contains hypophosphates, which are chemically capable of forming a chemical bond with the aluminum surface. This interaction results in the creation of a phosphate layer on the aluminum. This layer serves to improve the adhesion of the subsequent coating, which, in this case, is nickel phosphate. The chemical reaction between the hypophosphate and aluminum leads to the formation of Aluminum Hypophosphate. This Aluminum Hypophosphate layer acts as a primer, preparing the surface for the application of the nickel phosphate coating. This coating (pre-treatment) has a direct relationship with corrosion protection of alloy and in our case hypophosphite treatment was performed using the bath as mentioned in Table:

*Table 1. Chemicals and immersion parameters used for hypophosphite treatment*

<b>Hypophosphite Treatment</b>	
Sodium hypophosphite ( $NaH_2PO_2 \cdot H_2O$ )	30 g/L
Lactic Acid (80%)	20 $cm^3$ /L
pH	4.6
Temperature	85°C
Immersion Time	5 mins

### 3.3 Electroless Deposition – Coating Bath

In literature, there were found many coating baths but coating bath mentioned in Table 2 was found one of the simplest and suitable for Aluminum Coatings. All the materials were used of Analytical Grades and BN nanoparticles were of the size range from 75~100 nm.

*Table 2. Chemicals used for the electrolytic bath, its processing and optimized parameters*

Coating Bath and its Optimized Parameters	
Nickel Sulfate	28g/l
Sodium hypophosphite	30 g/l
Sodium Acetate	35 g/l
Lactic Acid (80%)	20 cm <sup>3</sup> /L
BN	0, 0.5, 1.0, 1.5, 2.0 %
pH	4.6
Temperature	85°C
Immersion Time	5 mins

### 3.4 Bath Composition:

EN plating is a crucial catalytic plating process widely used in commercial and industrial applications. Its significance lies in the exceptional properties of electroless nickel deposits, which depend on the composition of the EN coating. This composition, in turn, is influenced by the operating conditions of the EN deposition bath. Typically, an EN solution consists of several key components, including:

- A source of nickel ions
- A reducing agent
- Suitable complexing agents
- Stabilizers/inhibitors

- Energy

### 3.5 The Nickel Source:

The ideal source for nickel cations in EN plating is nickel sulfate. While other nickel salts like nickel acetate and have limited applications, they are not as commonly used. For example, nickel chloride can have detrimental effects when EN plating Al or when the EN deposit serves as a protective coating for iron-based alloys in corrosion-prone environments. The use of nickel acetate, though feasible, doesn't notably enhance bath performance or deposit quality when compared to nickel sulfate. Any slight advantages from nickel acetate are outweighed by its higher cost relative to nickel sulfate.

An idyllic source of nickel ions would be the nickel salt of hypo-phosphorous acid,  $\text{Ni}(\text{H}_2\text{PO}_2)_2$ . The use of  $\text{Ni}(\text{H}_2\text{PO}_2)_2$  offers the benefit of eliminating the need for sulfate anions while minimizing the accumulation of alkali metal ions. Additionally, it helps replenish the reactants that are consumed during the metal deposition process.

### 3.6 Reducing Agents:

Following are the four reducing agents in the EN plating process, and they share a structural similarity in that each contains more than two reactive hydrogens.

- Sodium hypophosphite  $\text{NaH}_2\text{PO}_2 \cdot \text{H}_2\text{O}$
- Sodium borohydride  $\text{NaBH}_4$
- Dimethylamine borane (DMAB);  $(\text{CH}_3)_2\text{NHBH}_3$
- Hydrazine  $\text{N}_2\text{H}_4 \cdot \text{H}_2\text{O}$

In our case, first one is the reducing agent of choice. The reduction of nickel is a result of the catalytic dehydrogenation of these reducing agents. Here's a summary of these nickel-reducing agents, which participate in the fundamental chemical reactions of the electroless nickel deposition:

Oxidation of the reducing agent:

Red - Ox +  $n\text{e}^-$

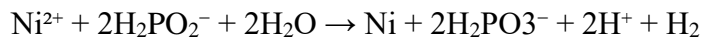
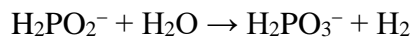
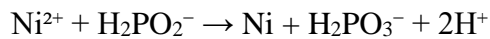


Reduction of nickel ions:



The reduction of nickel always goes hand in hand and evolve hydrogen. The coating formed is not pure Ni but rather contains additional elements like phosphorus or boron. This reduction reaction occurs exclusively on certain metal surfaces, and hydrogen ions are produced as a by-product. The utilization of the reducing agent for depositing metal is typically less than 100%, with the molar ratio of Ni deposited to reducing agent consumed usually equal to or less than 1.

Ni deposition using hypophosphite was once described in the literature with the equations mentioned below:



However, these equations fail to reason for the phosphorus constituent of the alloy in the deposit. Additionally, if the plating process followed these equations, the rate of deposition would be directly proportional to the reactant concentrations. Gutzeit has shown that in acid plating solutions (pH > 3.0), the plating rate has a first-order dependence on the hypophosphite concentration, meaning it varies significantly with hypophosphite concentration over a broad range. The rate is independent of the Ni ion content beyond approximately 0.02M Ni<sup>2+</sup>, indicating a zero-order dependence on Ni content. In alkaline solutions, the rate depends solely on the hypophosphite concentration.

Since the publication of Brenner and Riddell's paper in 1946, proposed four fundamental reaction mechanisms to explain EN deposition, as represented by stoichiometric reactions in previous equations. These mechanisms aim to elucidate nickel reduction by hypophosphite in both basic and acidic environments, accounting for the phosphorus component of the alloy. These mechanisms involve a secondary reaction of hypophosphite to elemental phosphorus and require a catalytic surface for the reaction sequence to proceed. Consequently, electroless nickel plating occurs exclusively on specific surfaces. It's worth noting that when steel or Al, two commonly

plated substrates, undergo EN plating, the initial phase involves a displacement reaction. In a surface reaction like electroless nickel deposition, the process unfolds in a series of consecutive steps:

- Diffusion of reactants ( $\text{Ni}^{2+}$ ,  $\text{H}_2\text{PO}_2^-$ ) to the surface
- Adsorption of reactants at the surface
- Chemical reaction on the surface
- Desorption of products ( $\text{HPO}_3^{2-}$ ,  $\text{HI}$ ,  $\text{H}^+$ ) from the surface
- Diffuse the products away from the surface

Above mentioned steps occur in sequence and step that is slowest of all is considered as rate determining step or factor. According to Brenner and Riddell, the Nickel is reduced because of atomic hydrogen which is formed via reaction between water and hypophosphite.

### 3.7 Substrate

Aluminum 7075 alloy has been chosen our case due to its vast applications in Aerospace and Automobile Industry. The chemical composition of the substrate under consideration is given in Table 3

*Table 3. Elemental composition of aluminum 7075 alloy*

Elements	Weight percentage
Zinc	5.1~6.1
Copper	1.2~2.0
Magnesium	2.1~2.9
Iron	0.19
Silicon	0.09
Titanium	0.02
Chromium	0.20

To examine the morphology of the materials, we utilized the JEOL-JSM-6490LA SEM, while FESEM analysis was conducted using the MIRA3 TESCAN instrument. Elemental composition was determined by employing an EDS detector attached to the FESEM.

### **3.8 Analysis and Characterization Techniques**

#### **3.8.1 Scanning Electron Microscopy (SEM):**

This advance imaging technique involves the precise focusing of a beam of electrons onto the surface of a specimen. This focused electron beam has the ability to dislodge photons or electrons from the material's surface. Subsequently, these dislodged electrons are collected and directed towards a detector. The information gathered by the detector is then used to control the brightness of a cathode ray tube (CRT).

The real power of SEM lies in its capability to generate high-resolution images of a material's surface. It predominantly relies on the detection of secondary electrons (SE) that are emitted from the vicinity of the sample's surface. This detection mode provides exceptionally clear and detailed images that can reveal features smaller than 1 nanometer in size. Apart from secondary electrons, backscattered electrons (BSE) are also generated as the incident electrons undergo elastic scattering. However, BSE originate from deeper within the sample, resulting in lower resolution images.

Moreover, SEM is equipped to detect characteristic X-rays produced when an inner shell electron is dislodged from its orbit, adding a chemical analysis dimension to its capabilities. This technique is highly valuable in material analysis due to its ease of sample preparation and the comprehensive insights it provides into a sample's morphology, chemistry, crystallography, and the orientation of crystal planes. SEM boasts adjustable magnification, offering a range from 10 to an impressive 500,000 times. This versatility makes SEM an indispensable tool for researchers and scientists across various fields.

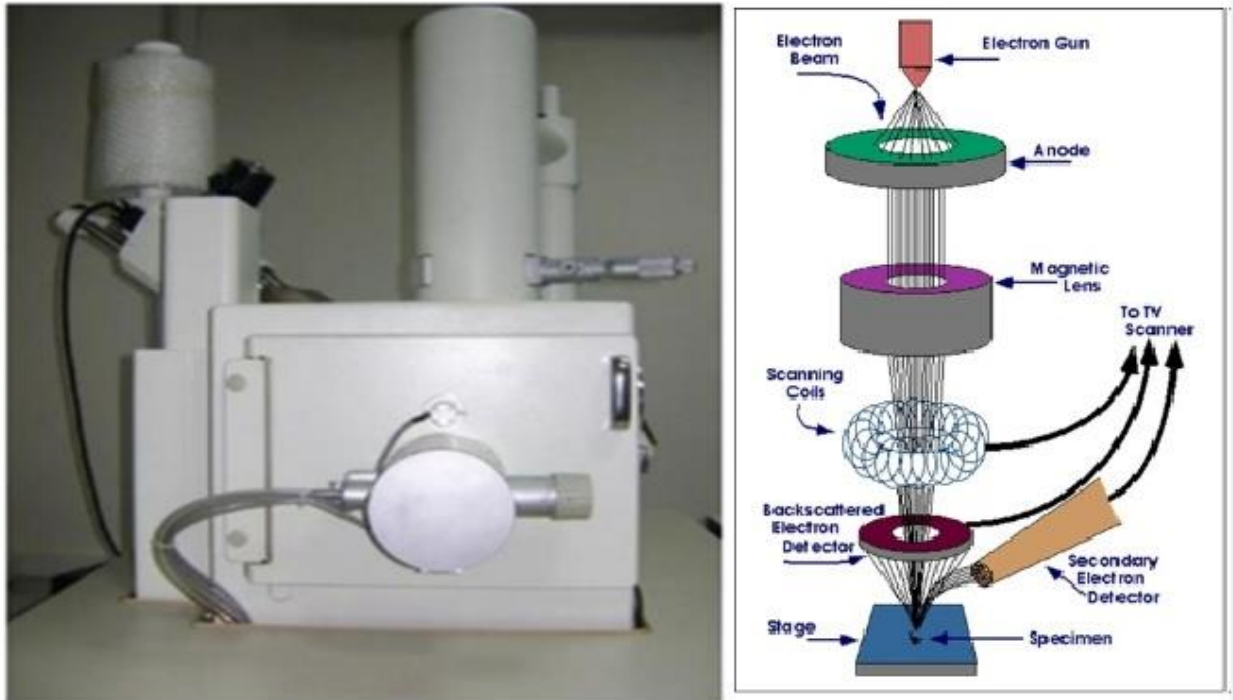


*Figure 6. Image of scanning electron microscopy, its mechanism and types of different rays involved during electron interaction with the sample [25]*

### **3.8.2 Energy Dispersive X-ray (EDX):**

Energy Dispersive X-ray Spectroscopy, often abbreviated as EDX or EDXRF (Energy Dispersive X-ray Fluorescence), is a highly valuable non-destructive analytical method employed to unveil the elemental composition of a given sample. It operates on a fundamental principle: when high-energy X-rays interact with a material, they have the capacity to displace inner shell electrons from the atoms within the sample. Subsequently, outer shell electrons shift to fill the voids left by the displaced inner shell electrons, emitting unique X-rays as they transition to lower energy states. These distinctive X-rays, specific to each element, serve as the cornerstone for elemental analysis using EDX.

The EDX process unfolds as follows:

- A source of high-energy X-rays, typically an X-ray tube, generates these X-rays, which are then directed toward the sample to be analyzed.
- The sample, meticulously positioned for examination, is often placed within a vacuum or low-pressure environment to ensure precise X-ray detection.

- The detector plays a pivotal role in capturing the emitted characteristic X-rays from the sample. Semiconductor detectors, like silicon drift detectors (SDD) or silicon drift chambers (SDC), are frequently chosen for their exceptional resolution and efficiency.
- The acquired X-ray spectra are subsequently processed and analyzed using specialized software.
- This software is critical for identifying and quantifying the elements present within the sample, based on the unique energies of the characteristic X-rays they emit.

### **3.8.3 X-Ray Diffraction (XRD):**

This technique is mainly used to analyze the crystal structure of the material and this is considered as one of the prime non diffraction characterization technique in Materials Sciences. It works by capturing the unique "fingerprints" of Bragg's reflections, which are indicative of crystalline substances. This method comprises three primary components: a cathode tube, sample holder, and detector. The process begins with the production of X-rays through the heating of a filament element, which propels electrons toward a target. These electrons collide with the target material. Crystals consist of intricate layers and planes. When X-rays with wavelengths resembling these crystal planes interact with the sample, they are reflected at an angle equal to the angle of incidence. This phenomenon is known as "diffraction" and is described by Bragg's Law:

$$2d\sin\theta = n\lambda\dots$$

When Bragg's law is satisfied, it signifies constructive interference, leading to the detection of "Bragg's reflections" by the detector. The sites/positions of these reflections provide data about inter-layer spacing. X-ray diffraction offers insights into a material's phase, crystallinity, and purity. Additionally, it can be used to determine lattice mismatch, the presence of dislocations, and unit cell dimensions.

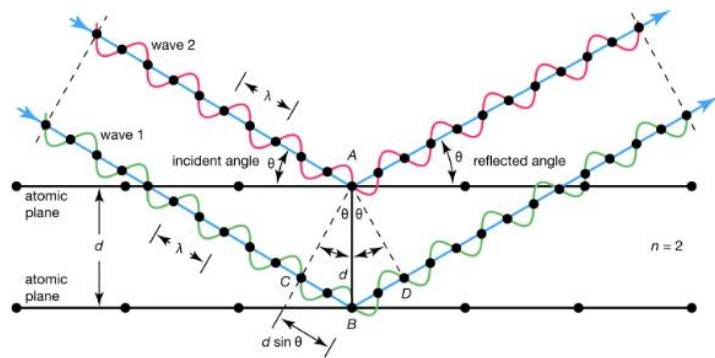
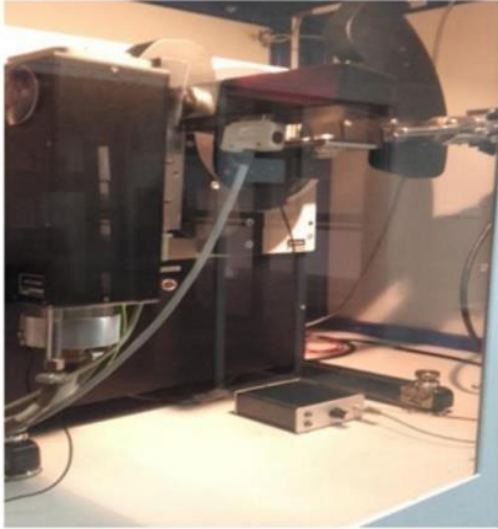


Figure 7. X-Ray machine and X-ray interaction with the atomic lattice, its mechanism and phenomena of the Bragg's law[28]

### 3.8.4 Atomic Force Microscope (AFM)

The Atomic Force Microscope (AFM) is a powerful tool that allows us to explore and understand the nanoscale world by measuring intermolecular forces and providing high-resolution imaging. It operates on three core principles: Surface Sensing, Detection, and Imaging.

**Surface Sensing:** AFM employs a sensitive cantilever with a sharp tip to scan the sample's surface. As the cantilever approaches, attractive forces draw it closer, causing deflection. Repulsive forces come into play when very close, leading to cantilever aversion.

**Detection:** A laser beam is directed onto the cantilever's surface. Changing deflection alters the laser's reflection angle, detected by a positive-sensitive photodiode (PSPD).

**Imaging:** AFM scans the cantilever across the sample's surface, and the deflection is monitored by the PSPD. A feedback loop maintains the cantilever's position, creating a precise topographical map.

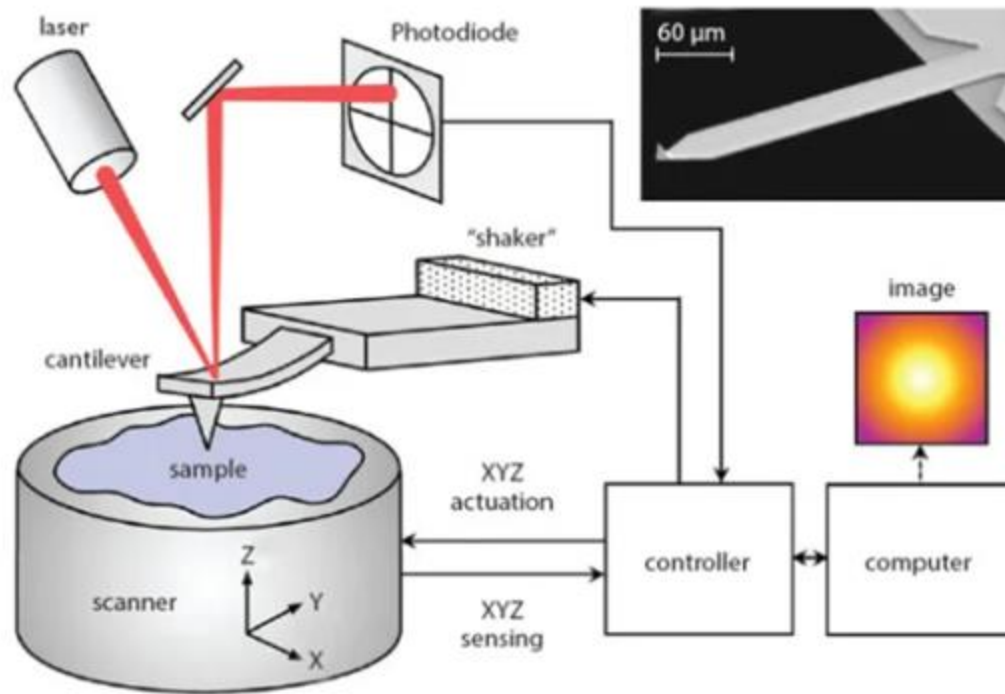


*Figure 8. Mechanism behind the atomic force microscopy. The interaction of the cantilever tip with the sample surface. Resultant data is collected by photodiode, from which computer forms an image [29]*

A fundamental aspect of AFM operation is the measurement of forces. The forces at play are calculated by determining the cantilever's stiffness and the amount of deflection. This calculation adheres to Hooke's law ( $F = -kz$ ), where  $F$  represents the force,  $k$  denotes the cantilever's stiffness, and  $z$  represents the distance by which the cantilever is bent. Accurate force measurements are essential for understanding the interactions and properties of the sample.

### **3.8.5 Microhardness – Vickers Hardness**

In the realm of materials science, understanding of mechanical properties of the material under use precisely become paramount. Vickers microhardness testing is a valuable tool for characterizing materials and solving complex engineering challenges. It employs a diamond indenter with a pyramidal geometry with an apex angle of 136 degrees. The Vickers indenter produces a square shaped indentation on the pre-prepared sample by applying external force, by which the indenter is pressed against the substrate for a specific dwell time. After removing the load, the size of the indent and the diagonals are measured using a microscope, and average

diagonal length (d) is used in calculations. The Vickers hardness number (HV) is determined using the formula:

$$HV = 1.8544 * (F / d^2)$$

where F is the force applied in kgf and d is the average diagonal length in millimeters.

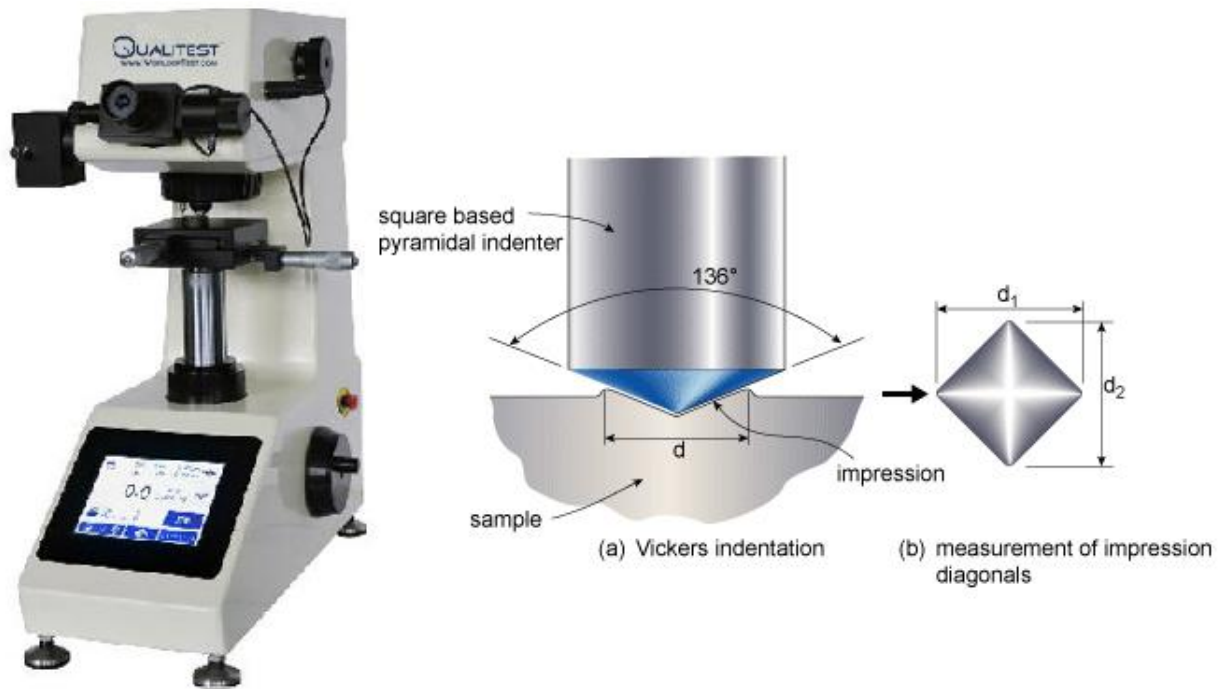


*Figure 9. The Vickers hardness tester and the indent measurement of the diamond shaped impression formed by the tip of the Vickers indenter [30]*

### **3.8.6 Tafel Scan**

Corrosion protective Ni-P coating are being extensively deployed in industries that uses metals as their prime raw material like automotive, construction and aerospace where corrosion resistance of the structure is critical. These coatings act as protective barriers against the environment extending the lifespan of the structures. To ensure the reliability of the structure, rigorous testing methods are required in which Tafel is the one through which one can get the valuable insights into the electrochemical behavior of coated samples.

#### **Principles of Tafel Scan Analysis**



Tafel scan analysis works on Tafel equation which follows the relationship between the current density and applied potential. Tafel equation can be expressed as:

$$i = B \exp(E/a)$$

where  $i$  represents current density, the constant  $B$  is related to the rate of electrochemical reaction,  $E$  is the external applied potential and  $a$  is the Tafel slope which relates to the reaction kinetics. In Tafel scans, the current density continuously measured against applied potential. The slope taken from the data obtained can give critical information about the corrosion behavior of a material for instance corrosion rate.

### **3.8.7 Electrochemical Impedance Spectroscopy (EIS)**

EIS is considered on the most utilized technique for the analysis pertaining to the electrochemical behavioral changes of the materials or system. This is not limited to simple electrochemical cells rather it also encompasses the complex interfaces / materials. EIS is a beneficial electrochemical testing which is used in the optimization of processes, coatings and energy storage system as it provides information regarding via analyzing electrical impedance over a range of frequency. The basic working principal of EIS is the impedance which is the opposition of the system towards applied alternate current (AC). Mathematically, impedance comprised of a magnitude (modulus) and phase:

$$Z = |Z| \exp(j\phi)$$

Where  $|Z|$  is the magnitude and  $\phi$  is the phase angle.



*Figure 10. Potentiostat interface instrument through which the EIS and potentiodynamic polarization measurements can be measured [31]*

Following are the main steps involved in EIS:

- Sample preparation
- Electrochemical cell setup
- AC signal application
- Impedance measurement
- Data analysis
- Model fitting

After sample preparation, an electrochemical cell setup is constructed which is comprised of the following

- Working Electrode
- Reference Electrode (Saturated Calomel Electrode)
- Counter Electrode

After the construction of electrochemical cell, AC voltage is applied to the working electrode and reference electrode serves as the reference potential over a range of frequencies. After applying AC voltage, response of the system is also observed via recording current and potential which further used to measure impedance at different frequencies. Then the data is analyzed via plotting Nyquist or Bode plots. Finally, the model fitting is carried out in which experimental data is fitted in a nearly similar electrical circuit model.

# Chapter 4

## Results and Discussion

### 4.1 XRD Analysis

XRD is utilized to determine the crystal structure and phases of the as-deposited coatings containing various concentration of phosphorous and BN nano-particles. Here the as-deposited structure of coatings containing P content from 8 to 11 wt% was investigated and prepared carefully by optimizing crucial bath parameters for instance, amount of hypophosphite in the electrolytic bath and current density. **Figure 11** represents the XRD pattern obtained for pure Ni-P coating, Ni-P with a pretreatment (i.e. hypophosphite treatment in our case) and hypo-phosphite pre-treated Ni-P with BN nano-particles reinforcement. Pure Ni-P and pretreated Ni-P coatings show the characteristic peak of (111) plane (ref # 98-007-6667) at  $2\theta$  equals to  $44.5^\circ$  which represents the FCC structure of Ni with a broad peak showing that with the inclusion of P in the Ni, the structure has distorted somewhat and the resultant structure obtained is not crystalline but amorphous. The inclusion of P in the Ni matrix making a Ni-P alloy described as a supersaturated solid solution in which P is dissolved in the crystalline Ni. Similar results have been reported for their as-deposited coatings that the incorporation of phosphorous atoms in the lattice of nickel changes the columnar structure to nodular grains which leads to the distortion of the Ni lattice. The XRD analysis of as deposited EN coatings shows the amorphous structure when the coatings are not post heat treated. This is also in consistence with the phosphorous content present in the deposits as can be seen in the later part of the dissertation. The XRD data is in good agreement with the data reported regarding Electroless Ni-P coatings with literature. It is generally perceived that with the inclusion of P with different concentrations, the crystallographic structure of Ni-P alloy changes and it transforms from crystalline to amorphous structure when the amount of P present in the alloy increases. The exact P content present in the alloy at which this transformation occurs is still unknown. It is also observed that with the incorporation of P in the Ni matrix, it broadens or widens the Ni peaks and make them less intense but will not affect the peak positions. This broadening of the Ni-P peaks indicates the decrease in the grain size as the P content increases

in the deposits. When the P content exceeds more than 9wt%, the only Ni (111) peak will appear and the rest of the peaks will disappear. This characteristic Ni (111) peak indicates an amorphous structure. The grain size measurement cannot be made possible above 9 wt% P content as the samples were made X-ray amorphous. When pre-treated Ni-P was reinforced with nanoparticles of BN, the XRD peak showed (002) plane at the low angle of  $2\theta$  at  $26.7^\circ$  (ref # 98-016-8892) which represented the presence of BN particles in the coatings. This confirms the successful incorporation of BN particles into the coatings. When the BN particles are incorporated, the heterogeneous nucleation takes place [29]–[31][9]. The low intensity of BN (002) can be linked with nickel peaks which are inherent and it can also be related to lower quantity of BN nanoparticles in NiP matrix. In literature, almost similar trend has been witnessed for the reinforcements used in small quantities [29], [30], [32], [33]. BN peaks at  $2\theta$   $41.7^\circ$  and  $50.2^\circ$  couldn't be identified because of amorphous Ni which blocks out the presences of other BN peaks. Also, the concentration of BN is low in the as deposited coatings when compared to Ni content. Hence, nickel peaks show high intensity compared to BN particles because of their low intensity in the coatings [34].

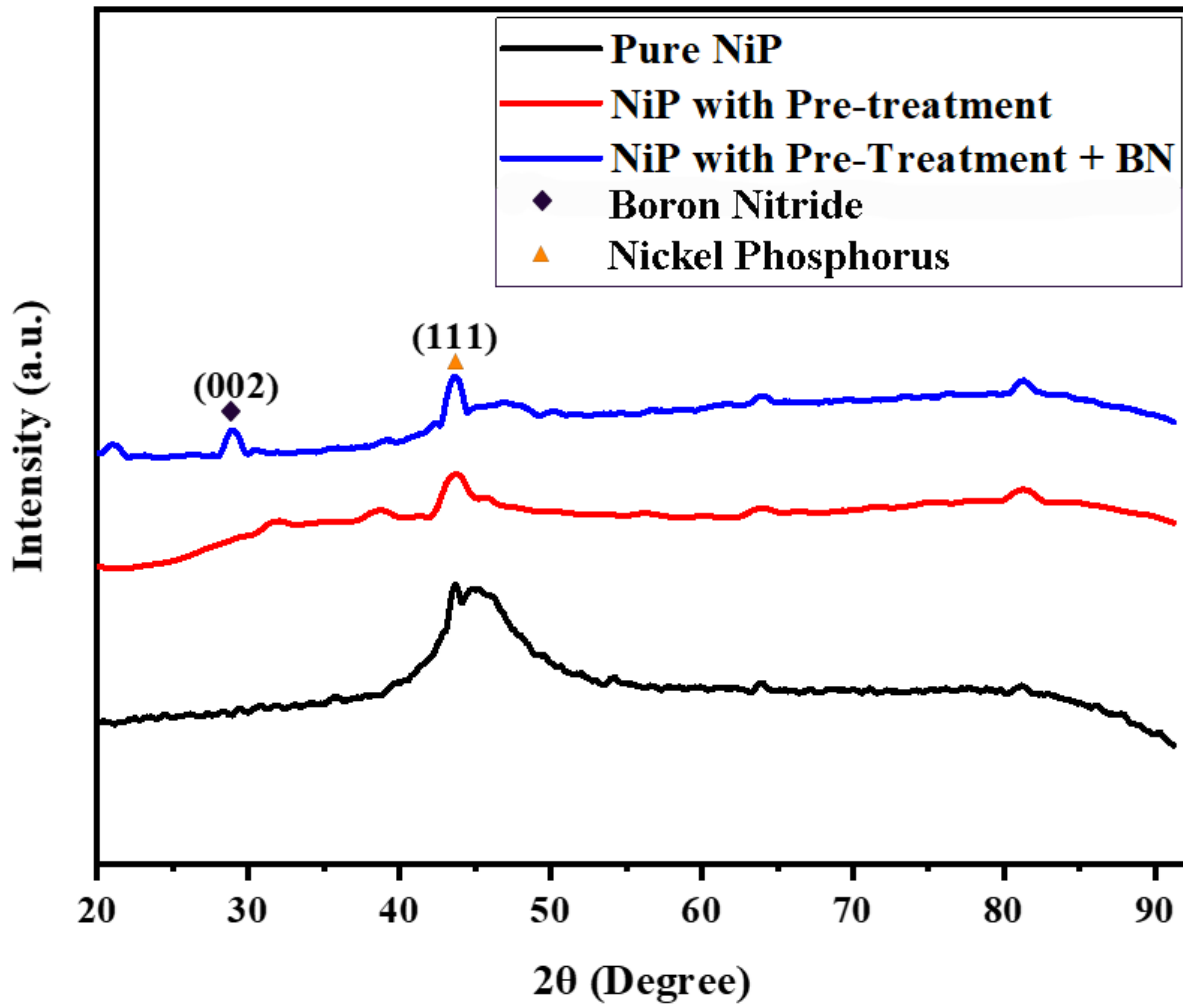
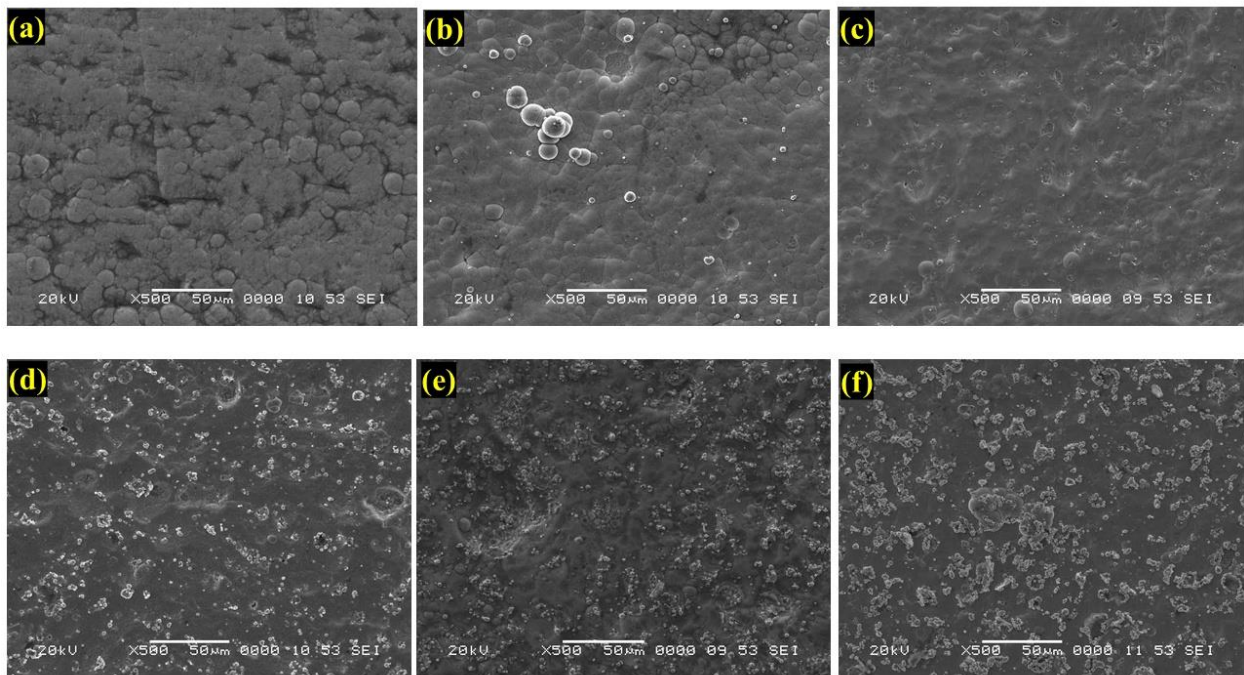


Figure 11. XRD peaks for with and without pretreatment and with BN reinforced Ni-P composite coatings.

## 4.2 SEM and EDS Analysis

SEM images reveals the morphological details of the coatings without any pre-treatment, with pretreatment (i.e., hypophosphite treatment in our case) and with BN reinforcements. **Figure 12** reveals that the Ni-P coatings had columnar like nodular structure for all the coatings. The coating without pre-treatment shows some dominant and larger nodules compared to coating with pre-treatment and the rest of the coatings. The coating with pretreatment effect shows some visible nodules as compare to the coating without pre-treatment, this has the effect on the hardness of the

coatings. Regarding the adhesion of the coating, the pretreatment provides more adhesion with the substrate as compared to the coating without pretreatment. This pretreatment also increases the P deposition in the resultant coatings – which again increases the hardness as we will see in the later sections of the manuscript. From the **Figure 12(c-f)** it can be seen that the morphology of the coatings has been changed with the inclusion of BN nanoparticles and this can be attributed to the heterogeneous nucleation sites provided by BN particles. As the concentration of BN increases to 1.0g/L, the morphology gets refined with smaller nodule sizes. This can be explained in a way that as the reinforcement is added to some concentration which is 1.0g/L in our case, the BN nanoparticles helped in lateral growth of the nickel matrix and provided new and more nucleation sites which results in the refined structure[35][36]. With further increase in the concentration of BN nanoparticles in the electrolytic bath, the deposited structure gets more refined as can be seen in the **Figure 12 (e and f)** having 1.5 and 2.0g/L BN concentration respectively. The overall coatings show a compact and homogenous structure with no cracks.



*Figure 12. SEM images of (a) without pretreatment of the Al substrate, (b) with pretreatment, (c) Ni-P/BN (0.5g/L), (d) Ni-P/BN (1.0g/L), (e) Ni-P/BN (1.5g/L), and (f) Ni-P/BN (2.0g/L) composite coatings*

**Figure 13** shows the cross-section of the Ni-P coating with the Al 7075 substrate. One can observe from the image that there is no void or cracks at the interface of the coating and the substrate. There is a well bonding and adhesion of the coating. This results in the high hardness of the coatings and good adhesion resist coatings from spalling off during the in-service conditions. The tape test was performed over the coatings and no pieces or chunks were found on the tape. The dark portion is representing the Al 7075 substrate and the brighter portion is showing the coating deposited on to the substrate surface. The average coating thickness was measured as  $11.8\mu\text{m}$  with standard deviation of  $\pm 1.34\mu\text{m}$ . **Figure 13** also presents a visual comparison of the samples with and without pre-treatment. This is clearly evident that in Figure 13 (a), there is not spalling off and coating is without porosity. However, breakage of coating is shown in Figure 13 (c) this also depicted in the hardness / corrosion results of the coating. This strong adherence (with the substrate) due to pre-treatment caused an increased electromechanical properties of the coating.

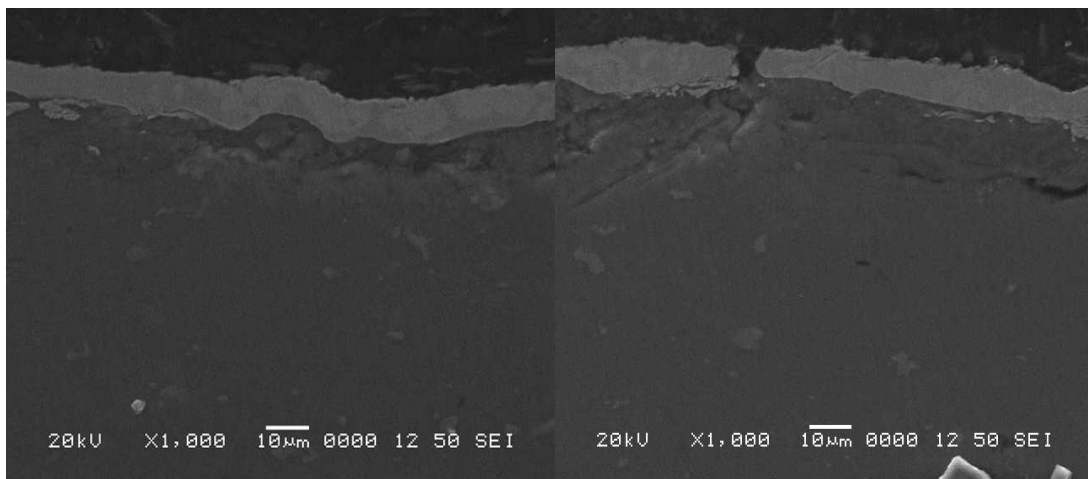


*Figure 13. SEM image of the cross-section of Ni-P coating, indicating the good adhesion of the coating with the substrate with Pre-Treatment and damaged / poor adhesion in without pre-treatment*

EDS analysis of the coatings has presented in the **Figure 13** and was applied on the coatings without pretreatment, with pretreatment of the substrate and with inclusion of BN nanoparticles. For clear evaluation and comparison, their compositional analysis is shown in the **Figure 13** which confirms that nickel and phosphorous both have deposited in the coating successfully along with boron and nitrogen. The values are presented in weight percentages. It can be noticed from the table that the coatings contain high phosphorous content which is mostly above 8 to 11wt% hence,



the structure would be fully amorphous which can also be confirm from the XRD given in the **Figure 11**. Coatings containing phosphorous content greater than 9wt% are considered to be high phosphorus which shows superior corrosion resistances. It can also be observed that as the concentration of BN increases in the bath, the BN content in the coatings also increases from 0.5g/L to 2g/L as reported by researchers. The B and N content seemed to increase from 1.75 to 3.56 at% and 4.08 to 12.34 wt% respectively. It can also be observed from the table that the deposition of BN takes place with expense of nickel meaning that as BN concentration increases, the nickel content in the coatings decreases[37]. Therefore, it can be said that the coatings contain high phosphorus content and inclusion of BN particles is not affect the P content or replaced the P content, rather the Ni content is decreasing. Hence, this results in the higher P content along with the high corrosion resistant properties[38][39]. From the EDX plot, the peak presented at 2keV is indicating the presence of phosphorous element. The peaks presented at around 0.8 and 7.5keV are for nickel element. The thickness of all the coatings were measured via SEM and the average thickness of coatings was came out to be 11 $\mu$ m.

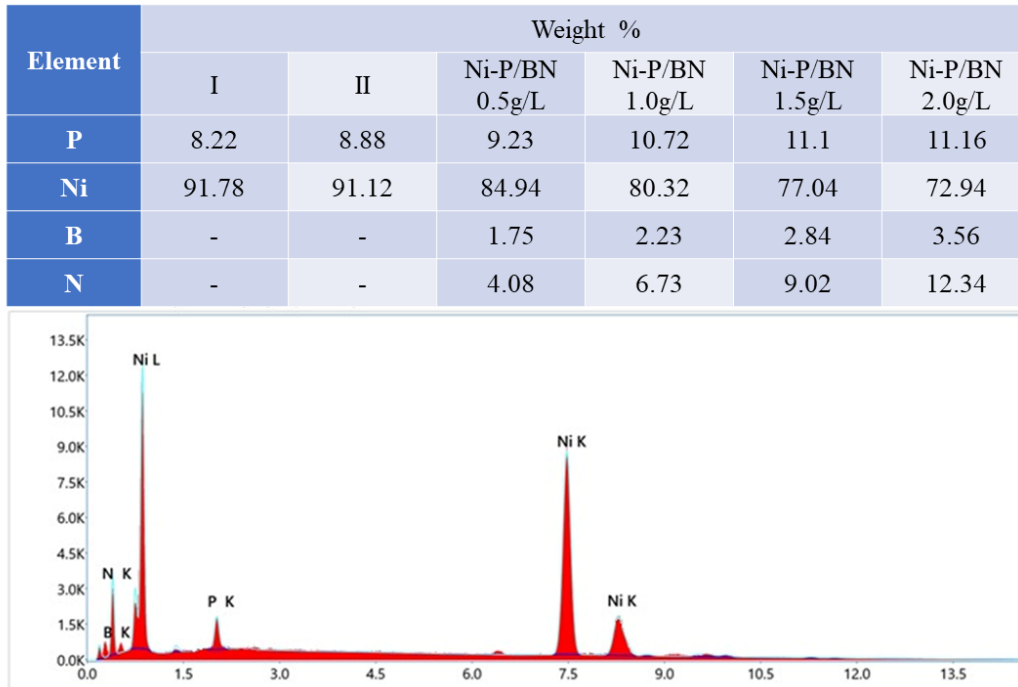


*Figure 14. EDX in wt% of without pretreatment of the Al substrate, with pretreatment, Ni-P/BN (0.5g/L), Ni-P/BN (1.0g/L), Ni-P/BN (1.5g/L), and Ni-P/BN (2.0g/L) composite coatings. EDX graph is presented at the bottom*

In the **Figure 14** the relationship between P content with time and coating thickness with time is given. The figure clearly explains that the phosphorus content is on higher side with an increase of coating time. The maximum P content reaches to 11.16wt% for 2.0g/L after the 90 minutes of the deposition time. The optimum coating obtained has the P content of 10.72wt% with 60 minutes of deposition time. It has nickel content of 80.32wt% and, B and N content of 2.23wt% and 6.73wt% respectively. During deposition of NiP coating, an analysis was carried out which as a part of coating optimization where a comparative analysis was performed with respect to coating thickness, phosphorus content and coating time in electroless coating bath. This analysis revealed that there is a direct relationship between coating thickness, Phosphorus content and coating time. In this analysis 05 samples were coated but they were removed from the coating bath after 30, 45, 60, 75 and 90 minutes of time interval. It was observed that coating achieved at 60 minutes was much better in terms of thickness, phosphorous content and surface uniformity.

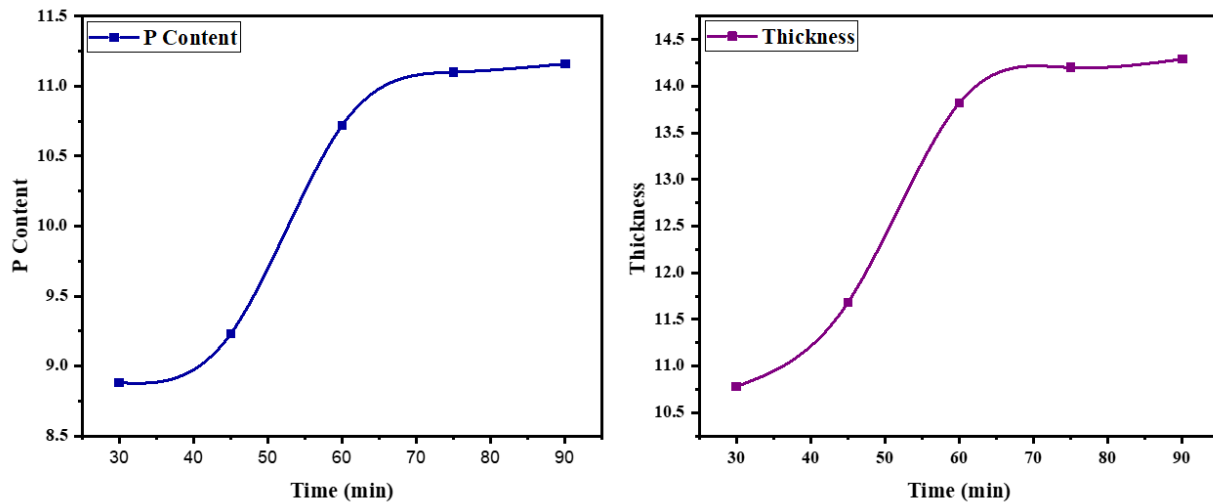


*Figure 15. Increase in the P content with deposition time (left), increase in the thickness of the coatings with increase in the deposition time (right)*

The **Figure 15** represents the relationship between hardness and the P content which is in weight percent. The trend seen in this figure shows that as the Pwt% content increases in the deposits, the

hardness of the coatings increases consistently. With the P content of 8.22, 8.88, 9.23, 10.72, 11.1, 11.16 wt%, the hardness of the coatings increases with the values of 416.80, 420.19, 651.85, 680.31, 735.47, 732.56 Hv respectively. This behavior is also observed by many other researchers as they reported that the increase in the P content results in the increase in the hardness.

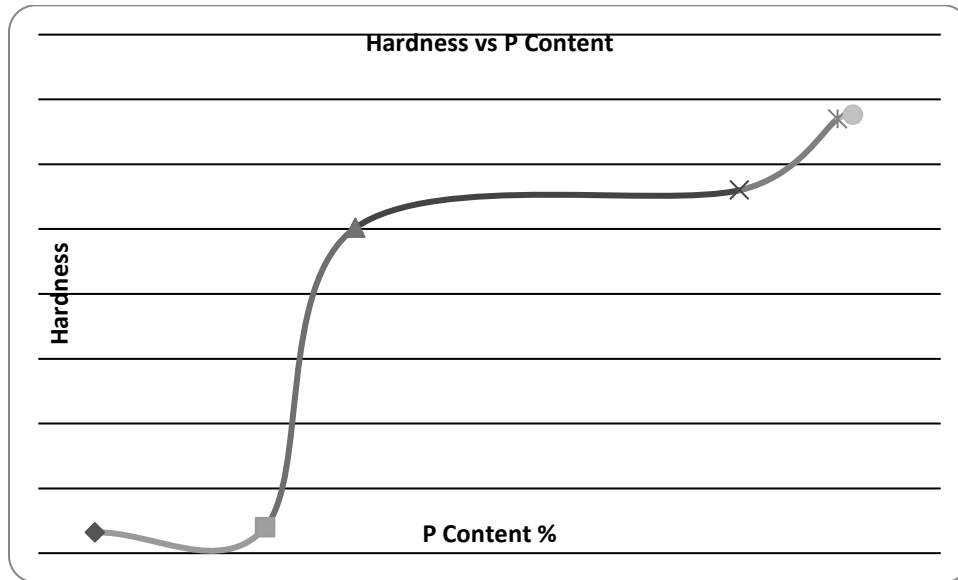


Figure 16. The relationship between P content in the deposits and their respective hardness values

### 4.3 AFM Analysis

The Atomic Force Microscopy (AFM) is used for the analysis of coatings with respect to their roughness mainly. Fig 15 depicts that the sample without any pre-treatment is smooth and fine. The coating with pre-treatment shows a bit higher surface roughness and this was due to the surface preparation and pretreatment with 50% HNO<sub>3</sub> to activate the surface. Further with the **Figure 15(c-f)**, The surface roughness of the coating (i.e., NiP) is increasing with an increased content of Boron Nitride nanoparticles in the electrolyte bath. This can be attributed to the reason that the BN particles are not soluble in the electrolyte and as they are hard particles incorporated in the Ni-P matrix. This is consistent with the other reported data [40][41]. Also, this extensive increase in surface roughness is because of the agglomeration of the BN particles as their concentration increases above the optimization concentration in the bath from 1.0g/L up to 2g/L.

Additionally AFM also reported that the coating is devoid of any defects, cracks or pores having uniform homogeneity.

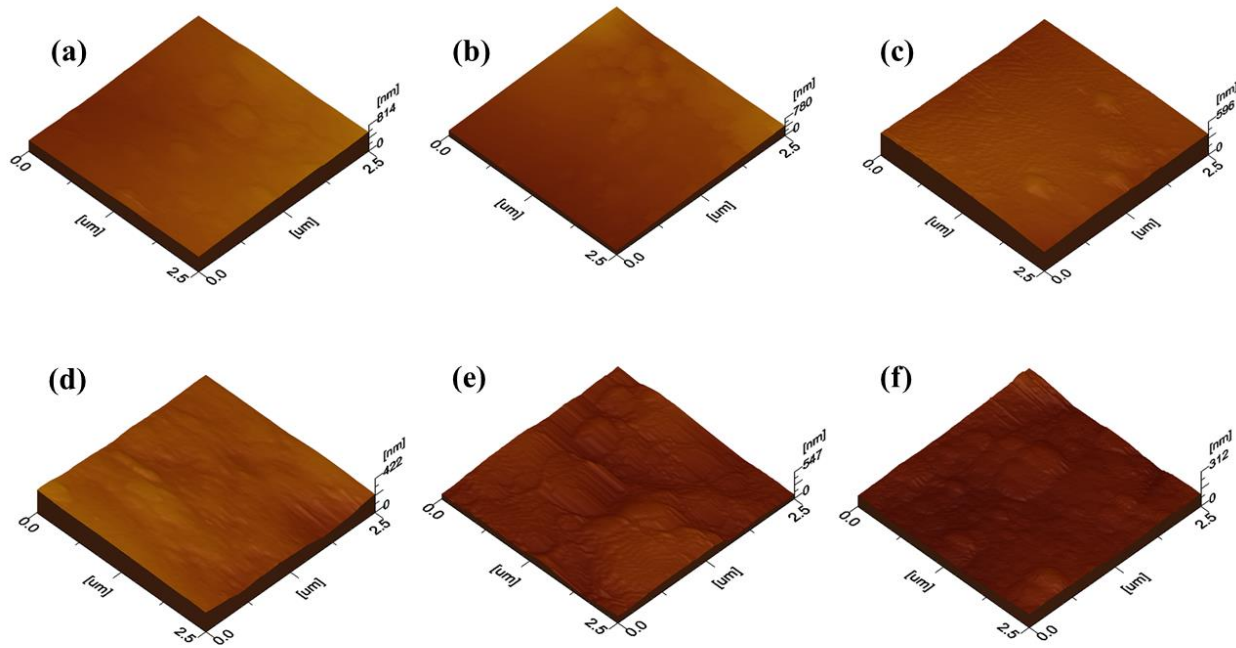


Figure 17. AFM images of (a) without pretreated Al substrate, (b) with pretreatment, (c) Ni-P/BN (0.5g/L), (d) Ni-P/BN (1.0g/L), (e) Ni-P/BN (1.5g/L), and (f) Ni-P/BN (2.0g/L) composite coatings.

Table 4. Roughness values obtained from AFM along with their avg. deviation

Sample Name	Roughness Ra (nm)
Ni-P Without Pretreatment	$9.91 \pm 0.23$
Ni-P with Pretreatment	$15.3 \pm 0.85$
Ni-P/BN (0.5g/L)	$29.1 \pm 0.46$
Ni-P/BN (1.0g/L)	$45.0 \pm 0.67$
Ni-P/BN (1.5g/L)	$53.2 \pm 0.94$
Ni-P/BN (2.0g/L)	$59.8 \pm 0.34$

The agglomeration occurs due to the greater surface energies of BN nanoparticles as well as the decrease in the distance between the particles which results in more attractive forces between them which results in the formation of agglomerates. This agglomeration of nanoparticles can cause the deterioration of the mechanical, wear and corrosion resistant properties when a certain level is

crossed. In our case, it is observed that maximum surface roughness is increase till 1.0 g/L. This is also observed in the corrosion / hardness results which clearly shows that linear increase in properties got disturbed with addition of BN nanoparticles above 1.0 g/L.

#### 4.4 Micro-hardness

The microhardness – Vickers hardness of electroless binary Ni-P alloy coating and Ni-P/BN composite coating with a load of 100g is presented in the tabular form in **Table 5**. The Vickers hardness was evaluated for the coatings containing 0.5, 1.0, 1.5, 2.0 g/L BN nanoparticles and their respective microhardness comes to be 651.85, 680.31, 735.47 and 738.56 HV respectively. It was observed that the values of microhardness of all the composite coatings is higher than the simple Ni-P coatings, either they are deposited with or without pretreatment. It can be noted that the coating with lower BN particle concentration is less hard than with the coatings containing higher amount of BN concentration. Generally, the strengthening mechanism of the metals and alloys described by the researchers is as follows:

- (i) dispersion hardening/strengthening – Orowan mechanism
- (ii) grain refinement strengthening as described by Hall-Petch relationship
- (iii) crystal orientations and finally
- (iv) by solid solution strengthening.

In our case the, the improvement in the hardness of Ni-P to Ni-P/BN composite coatings can be explained on the behalf of BN nanoparticles distributed in the Ni-P matrix which helps in restraining the lateral growth of the matrix and also restrains the plastic deformation of the matrix under certain load because of the grain refinement and dispersive strengthening effects. The uniformity of the structure also plays an important role in the high hardness but is less significant in the nanocomposite coatings where the contribution from dispersion strengthening overcomes the other facts because of the uniform distribution of BN nanoparticles.

Mechanical properties of with and without pretreated coatings and with various concentrations of BN nanoparticles were evaluated through microhardness – Vickers hardness technique. **Table 5** shows the average hardness values of all the coatings. The microhardness of binary Ni-P coating

without pretreatment of the aluminum substrate is around 416.80 HV<sub>0.1</sub>. In contrast, the Ni-P coating with pretreatment, the hardness value increases to 420.19 HV<sub>0.1</sub>. This increase in hardness with pretreatment is due to the better adhesion of the coating with the substrate and less roughness. Also, this is because the P content increases from 8.22wt% to 8.88wt% when the substrate is pretreated. Hence, as the P content increases, the hardness and also the corrosion resistant properties also increase. When the composite coatings are under consideration, the hardness values increase up to 738.56HV<sub>0.1</sub>.

*Table 5. Vickers hardness data and nanoindentation hardness data of without pretreatment, with pretreatment and Ni-P/BN composite coatings*

<b>Sample Name</b>	<b>Hardness Hv<sub>(0.1)</sub></b>	<b>Hardness (GPa)</b>
Ni-P Without Pretreatment	416.80±0.15	4.08 ± 0.61
Ni-P with Pretreatment	420.19±0.76	4.12 ± 0.23
Ni-P/BN (0.5g/L)	651.85±0.42	6.39 ± 0.34
Ni-P/BN (1.0g/L)	680.31±0.67	6.67 ± 0.93
Ni-P/BN (1.5g/L)	735.47±0.91	7.21 ± 0.56
Ni-P/BN (2.0g/L)	738.56±0.68	7.24 ± 0.28

The hardness increases due to the following factors: i) compact and homogeneous structure, ii) solid solution strengthening, iii) dispersion hardening etc. It can be observed that all the factors are followed by the coating possess 1.0g/L BN nanoparticles. The BN particles seem to be dispersed homogeneously all over the coating with no agglomeration which assists in increase in the hardness of the coating. Also, as the nodular size decreases, their grain boundaries provide barrier to the dislocation movements and hence making the structure resistant to plastic deformation.

To complement the Vickers hardness testing results and also to verify them, nano-indentation tests were performed for the coatings without pretreatment, with pretreatment and with BN reinforcements. From the graphs presented in the **Figure 16**, it can clearly be seen that the graphs

are shifting towards left and the indentation depth for all the reinforcements is reducing leading to improved hardness of all metallic-composite coatings.

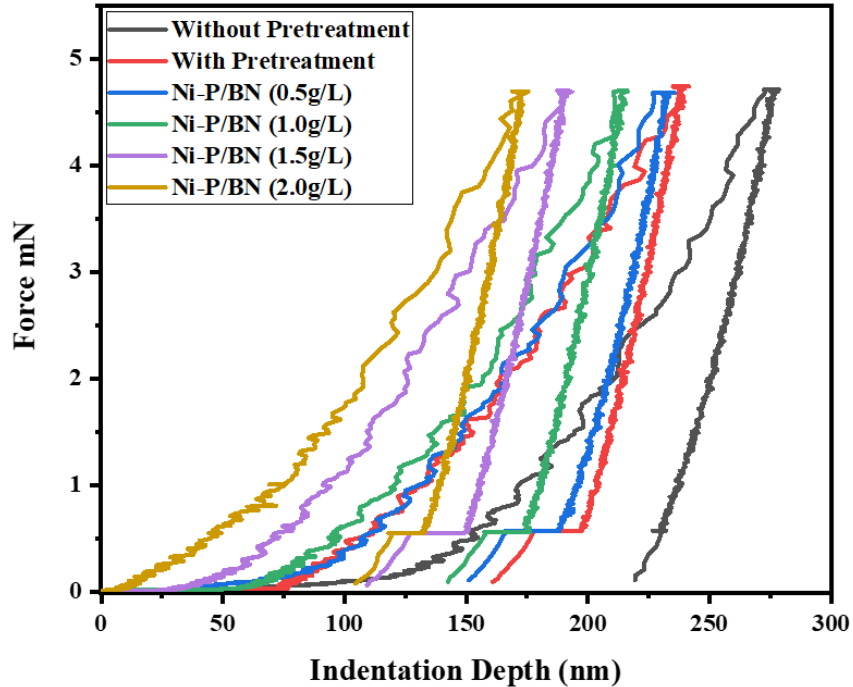


Figure 18. Nanoindentation graphs of (a) without pretreated Al substrate, (b) with pretreatment, (c) Ni-P/BN (0.5g/L), (d) Ni-P/BN (1.0g/L), (e) Ni-P/BN (1.5g/L), and (f) Ni-P/BN (2.0g/L) composite coatings

The coating without pretreatment has the hardness of 4.08GPa and when the substrate is treated with 50% solution of  $\text{HNO}_3$  the hardness rises to 4.12GPa and a gradual increase in hardness was seen with the increase in reinforcement of BN nanoparticles from 0.5g/L to 2.0g/L. the hardness with 0.5g/L BN was 6.39GPa and it increases to the maximum value of 7.24GPa when the reinforcement was increases to 2.0g/L. This increase in hardness elaborates the idea of protecting the substrate from external scratch and when seen microscopically it provides the protection against plastic deformation and BN supports in inhibiting the movement of dislocations which results in dispersion hardening. The phenomena of dispersion hardening takes place when the nano-reinforcements are dispersed in the coatings homogeneously and in result it boosts the load endurance capacity of the structure/coating. As the ceramic particles are hard enough, they don't

break or deform when the crack propagates and hence it changes the crack propagation path by acting as obstacle to the cracks and deformation.

#### 4.5 Corrosion Analysis – EIS and Tafel Plots

EIS stands for Electrochemical Impedance Spectroscopy and is widely utilized in order to study the corrosion resistance mechanism of a system. **Figure 17** shows the fitted bode plots ((a) phase angle vs log(f) and (b) log |Z<sub>i</sub>| vs log(f)) of without pretreatment, with pretreatment and with BN nano-reinforced coatings. **Figure 18** shows the equivalent electric circuit implemented for data fitting such that its according to Randle cell for the aluminum substrate and cascaded two-time constant circuit was used for with and without pretreated sample and also for those samples with BN reinforcement. Electrical elements which were used for fitting were:

R<sub>s</sub>: Solution resistance

R<sub>ct</sub>: Charge transfer resistance

R<sub>po</sub>: Pore resistance of the coating

CPE1 and CPE2: Constant phase elements which act as a capacitor indicating any inhomogeneity obtained as a result of the equation below:

$$1/Z_{CPE} = Q(j\omega)^n$$

Where Q represents the admittance, j itself is the imaginary number, ω is the angular frequency produced by AC signal and n is the CPE exponent. When the value of n = 1, element acts like a pure capacitor. When value of n is 0, element acts purely like a resistor. And when n is greater than 0 and less than 1, the element behaves like I has been deviated from the ideal behavior.

Phase angle vs log of frequency response of all the coatings are presented in the **Figure 17(a)**. The phase angle of aluminum 7075 substrate is narrowed in the mid-frequency region which represents the single time constant. The shift in the phase angle vs log(f) from mid-frequency region to high frequency region along with the broadness of the curve reveals the presence of cascaded two time constant for BN reinforced Ni-P coatings. **Figure 17(a&b)** shows the impedance response of the with and without pretreated and with BN reinforced composite coatings and the increase trend in the impedance shows that the protective hypophosphite layer has been formed which helps in



impeding the corrosion of the coatings as also reported in literature [42][43]. Moreover, the inclusion of BN nanoparticles in the electrolyte, help in filling the micropores and voids during their deposition along with the Ni-P matrix, resulting enhanced resistance towards corrosion. Hence, their increased amount in the as deposited coatings, as they are inert particles, further increase the overall impedance as they impede the corrosion initiation sites. This also results in the increase in the charge transfer resistance  $R_{ct}$ , as the BN concentration increases. This is because they conceal the corrosion active area and restricts the movement of electrons from the electrolyte towards the aluminum substrate as also explained in literature [44][43].

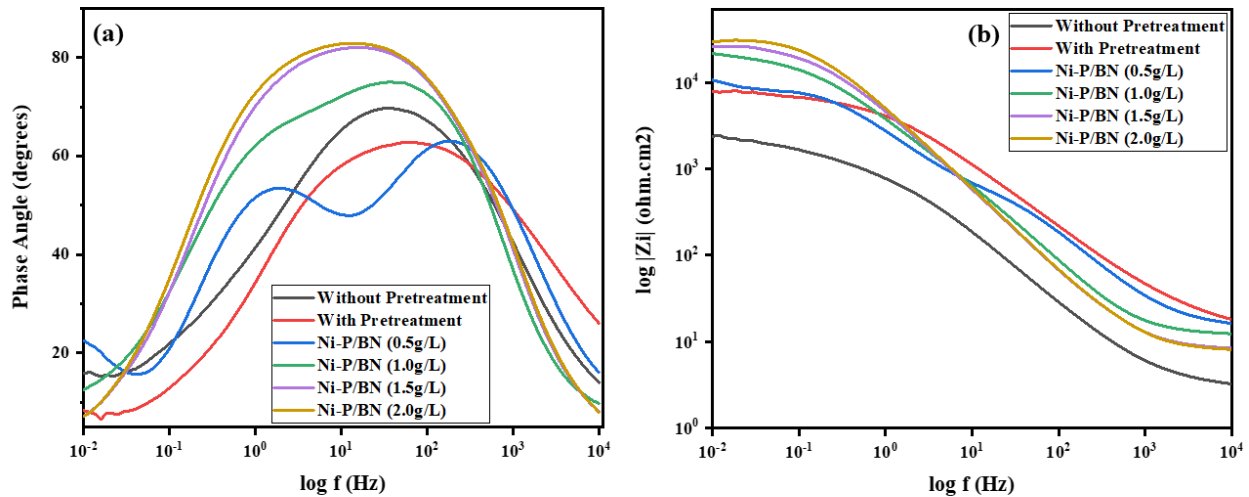


Figure 19. Bode plots. (a) Phase angle vs  $\log(f)$ . (b)  $\log |Z_i|$  vs  $\log(f)$  of without pretreated Al substrate, with pretreatment, Ni-P/BN (0.5g/L), Ni-P/BN (1.0g/L), Ni-P/BN (1.5g/L), and Ni-P/BN (2.0g/L) composite coatings

Nyquist plots show impedance of the coatings. These electrochemical impedance measurement/values are most important/useful and informative regarding measuring the corrosion of the films deposited on the conductive substrates. This technique is basically having the capability to work in situ and is non-destructive probe relaxation phenomena which works over the wide range of frequency.

The Nyquist plots presented in the **Figure 19** represents the impedance trend of the coatings as also be described by Bode plot in the **Figure 17**. The consecutive rise in the impedance is shown by increase in the diameter of the semi-circular loop and this increase is due to the addition of BN nanoparticles in the Ni-P metal matrix. The highest value of impedance obtained was of the coating with 2.0g/L BN particles. The values of  $R_{po}$  and  $R_{ct}$  when compared reveals that both the pore resistance and charge transfer resistance got improved because of incorporating inert ceramic particles into the Ni-P alloy matrix. The corrosion enhancement primarily can be attributed to i) number of pores exhibited by Ni-P matrix and ii) decrease in the contact area of the chloride ions present in the electrolyte with the Ni-P/BN surface.

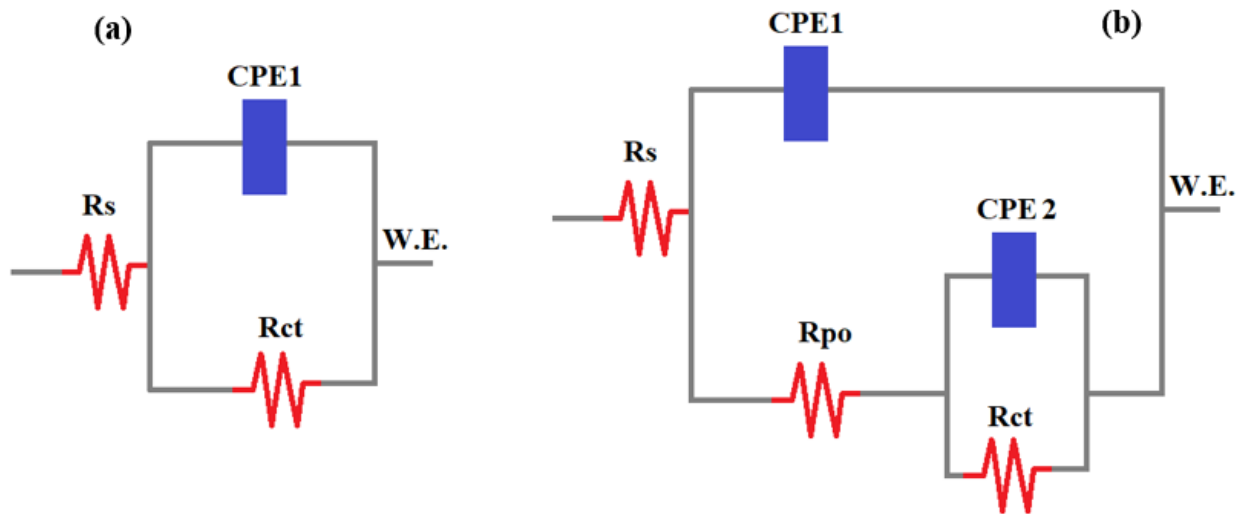


Figure 20. Circuit diagrams for EIS fitting of (a) without and with pretreated Ni-P coating and (b) without and with pretreated Ni-P/BN with different concentrations of BN reinforcements.

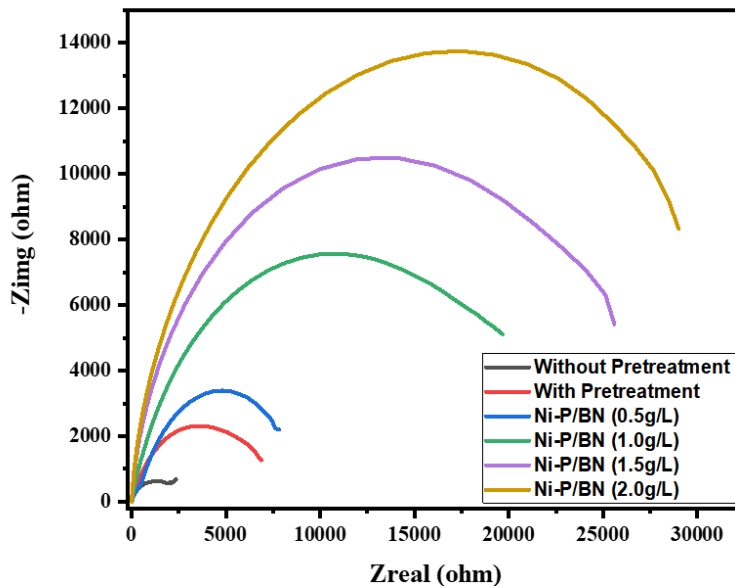
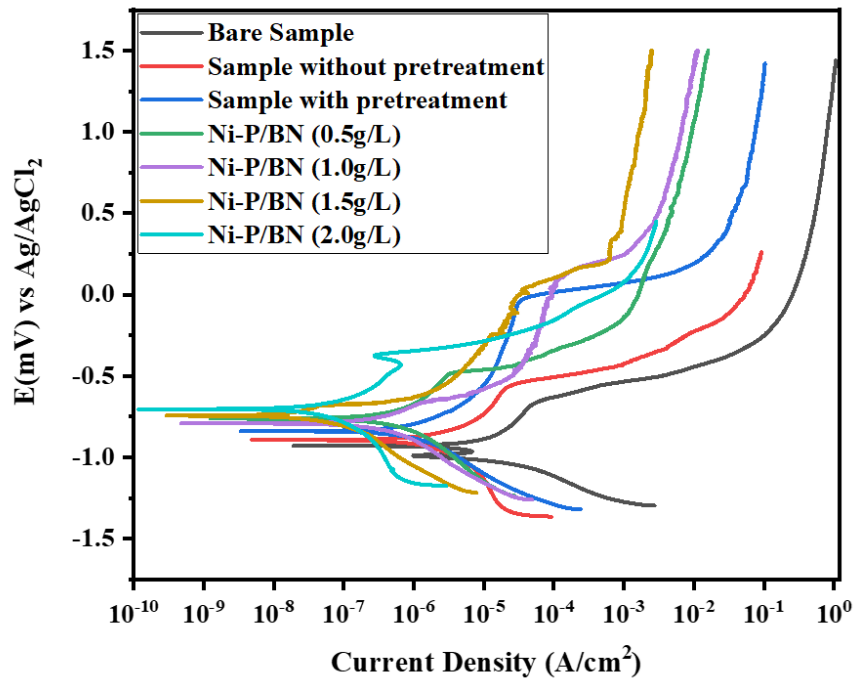


Figure 21. Nyquist plot of without pretreated Al substrate, with pretreatment, Ni-P/BN (0.5g/L), Ni-P/BN (1.0g/L), Ni-P/BN (1.5g/L), and Ni-P/BN (2.0g/L) composite coatings

The OCP of the samples measured in 3.5% NaCl solution is measured and all the potentials were measured against Ag/AgCl<sub>2</sub> electrode. The variation of potential shows that it varies continuously and attain a constant value after around 30 minutes of the run test. This change in the potential shows the nobleness of the coatings. The OPC of the bare Al substrate found to be most negative value but the OCP of the Ni-P coating containing 2.0g/L BN incorporated coating shows the largest shift in the OCP values which shifted towards more positive values of the potentials which reflects the most stable/noble character in 3.5% NaCl solution.

The potentiodynamic polarization experiments which were carried out in 3.5% NaCl solution for the coatings and **Figure 20** shows the Tafel plots of the coatings without pretreatment, with pretreatment and with inclusion of BN nanoparticles. Corrosion characteristics for instance OCP measurements for alloy and composite coatings, Tafel plots, potential  $E_{\text{corr}}$ , corrosion current density  $i_{\text{corr}}$ , corrosion rate (CR) and finally anodic and cathodic slopes for all the coatings can be obtained by using Stern-Geary relationship. This can also be obtained from Tafel plots by extrapolating method.

The **Figure 20** reveals that the graphs shifted from right to left which means the current density decreases with regard to bare aluminum substrate when the BN particles are added. Current density decreases for all the samples without and with-pretreated samples and with BN particles. Similarly, the graphs shifted from negative potential to positive potential. In other words, it shifted from upwards which represents the stability of the coatings with respect to their environment. The results of potentiodynamic polarization are presented. The  $E_{\text{corr}}$  presented the same trend as that of the  $i_{\text{corr}}$  for the clear comparison, the  $E_{\text{corr}}$  and  $i_{\text{corr}}$  values are presented in the **Table 5**. The highest current density of about  $35.42\mu\text{A}/\text{cm}^2$  can be observed for the bare Al substrate and it further decreases to  $1.33\mu\text{A}/\text{cm}^2$  for 2.0g/L BN particles, which tells an improved corrosion resistances of the coatings containing BN reinforcements. By comparing the values, it is obvious that the increase in BN concentration will lead to an improved corrosion resistance, as they are inert and insoluble and they also reduced the active areas and blocks the pathway between the electrolyte and the substrate as described by other researchers [43][44].



*Figure 22. Tafel plots of bare Al substrate, without pretreated Al substrate, with pretreatment, Ni-P/BN (0.5g/L), Ni-P/BN (1.0g/L), Ni-P/BN (1.5g/L), and Ni-P/BN (2.0g/L) composite coatings*

The results indicate that the  $E_{\text{corr}}$ , which is also known as corrosion potential, of the bare Al sample is the most negative -0.9289 mV. It was observed that the incorporation of BN nanoparticles results in shifting the  $E_{\text{corr}}$  to positive values and the highest positive value is obtained for Ni-P/BN (2.0g/L) composite coating and the highest value reaches up to -0.7620 mV. The anodic and cathodic slopes for all the coatings were different by themselves as well as from bare Al substrate. The  $I_{\text{corr}}$  value decreases and potential values increases for the coatings containing BN nanoparticles ranging from 0.5 to 2.0g/L concentration. The composite coating with higher BN concentration doesn't show much increase in  $I_{\text{corr}}$ . This may be due to reaching the maximum extent of incorporating BN particles where further increase in concentration doesn't affect much of the corrosion resistant properties of Ni-P coatings. It can also be observed from the polarization data that incorporation of BN in Ni-P coating most likely influence the kinetics of both anodic and cathodic electrochemical reactions.

*Table 6.  $I_{\text{corr}}$  and  $E_{\text{corr}}$  data of without pretreatment, with pretreatment and Ni-P/BN composite coatings obtained from Tafel curves*

<b>Sample Name</b>	<b><math>I_{\text{corr}} \mu\text{A}/\text{cm}^2</math></b>	<b><math>E_{\text{corr}}</math> (mV)</b>
Bare Aluminum Sample	35.428	-0.9289
Sample without Pretreatment	28.367	-0.8938
Sample with Pretreatment	14.815	-0.8406
Ni-P/BN (0.5g/L)	8.619	-0.7892
Ni-P/BN (1.0g/L)	3.163	-0.7030
Ni-P/BN (1.5g/L)	1.434	-0.7283
Ni-P/BN (2.0g/L)	1.336	-0.7620

It is observed by the researchers that for the coatings showing superior corrosion resistance should have properties like uniform homogeneous surface with no cracks and pores, and also the elements should be evenly distributed in the alloy.

## Conclusions

This thesis comprehensively explores the comparison of the substrate with and without pretreated aluminum 7075 substrates deposited with Ni-P alloy coating. The impact of nano reinforced BN particles on mechanical and corrosion resistant properties were also studied with different concentrations of BN (0.5, 1.0, 1.5, 2.0) g/L forming the composite Ni-P/BN coatings.

The extensive analysis of various coatings has unveiled the outstanding enhancement in the mechanical and corrosion resistant properties. The coatings possess nodular morphology with well adhesion with the Al substrate. All the coatings studied were free of cracks and pores. When the p content in the coatings and coating thickness was plotted against time, it was observed that the P content increases drastically till 75 minutes of deposition then it gets constant. Similarly, the thickness of the coatings increases till 75 minutes of time then it gains the constant value. From the AFM analysis it was observed that the roughness of the coatings enhanced continuously as the BN concentration increases in the electrolytic bath. The maximum roughness reached to 59.8nm. The micro-Vickers hardness and nanoindentation results showed the continuum increase in the hardness of the Ni-P/BN composite coatings. The coating with 2.0g/L BN nanoparticles boasted the performance of the coatings in terms of hardness as well as in protecting the coating from corrosion. The maximum hardness reached to the value of 7.24 GPa and the minimum  $i_{\text{corr}}$  was reached to  $1.136 \mu\text{A}/\text{cm}^2$ . The Nyquist as well as the Bode data for the Ni-P/BN (2.0g/L) showed remarkable resistance to corrosion.

Overall, the coating with 2.0g/L BN can be applied where hard and corrosion resistant properties of Al structures are required. Hence, this work offers valuable perspective regarding crafting and advancing high-quality coatings that can be applied in diverse engineering applications.

## References

- [1] H. Mindivan, "Tribocorrosion behavior of electroless Ni-P/Ni-B duplex coating on AA7075 aluminum alloy," *Ind. Lubr. Tribol.*, vol. 71, no. 5, pp. 630–635, 2019, doi: 10.1108/ILT-05-2018-0177.
- [2] W. Qin, "Microstructure and corrosion behavior of electroless Ni-P coatings on 6061 aluminum alloys," *J. Coatings Technol. Res.*, vol. 8, no. 1, pp. 135–139, 2011, doi: 10.1007/s11998-010-9256-3.
- [3] J. Musil and J. Vlček, "Magnetron sputtering of hard nanocomposite coatings and their properties," *Surf. Coatings Technol.*, vol. 142–144, pp. 557–566, 2001, doi: 10.1016/S0257-8972(01)01139-2.
- [4] J. G. Kim, A. C. Frenkel, H. Liu, and R. M. Park, "Growth by molecular beam epitaxy and electrical characterization of Si-doped zinc blende GaN films deposited on  $\beta$ -SiC coated (001) Si substrates," *Appl. Phys. Lett.*, vol. 65, no. 1, pp. 91–93, 1994, doi: 10.1063/1.113085.
- [5] J. L. Mo, M. H. Zhu, B. Lei, Y. X. Leng, and N. Huang, "Comparison of tribological behaviours of AlCrN and TiAlN coatings-Deposited by physical vapor deposition," *Wear*, vol. 263, no. 7-12 SPEC. ISS., pp. 1423–1429, 2007, doi: 10.1016/j.wear.2007.01.051.
- [6] R. Gordon, "Section 3. Glass coating at atmospheric pressure: Chemical vapor deposition of coatings on glass," *J. Non. Cryst. Solids*, vol. 218, pp. 81–91, 1997, doi: 10.1016/s0022-3093(97)00198-1.
- [7] J. T. S. Irvine, T. Politova, and A. Kruth, "Yttria co-doping of scandia-zirconia electrolytes for SOFCs," *Proc. - Electrochem. Soc.*, vol. PV 2005-07, no. September 2001, pp. 941–946, 2005, doi: 10.1149/ma2005-01/30/1137.
- [8] T. S. Sidhu, S. Prakash, and R. D. Agrawal, "Studies on the properties of high-velocity oxy-fuel thermal spray coatings for higher temperature applications," *Mater. Sci.*, vol. 41, no. 6, pp. 805–823, 2005, doi: 10.1007/s11003-006-0047-z.
- [9] R. M. H. Pombo Rodriguez, R. S. C. Paredes, S. H. Wido, and A. Calixto, "Comparison of

- aluminum coatings deposited by flame spray and by electric arc spray,” *Surf. Coatings Technol.*, vol. 202, no. 1, pp. 172–179, 2007, doi: 10.1016/j.surfcoat.2007.05.067.
- [10] P. Sharma, S. P. Singh, S. K. Parakh, and Y. W. Tong, “Health hazards of hexavalent chromium (Cr (VI)) and its microbial reduction,” *Bioengineered*, vol. 13, no. 3, pp. 4923–4938, 2022, doi: 10.1080/21655979.2022.2037273.
- [11] Y. Liu, J. M. C. Mol, and G. C. A. M. Janssen, “Combined Corrosion and Wear of Aluminium Alloy 7075-T6,” *J. Bio- Tribo-Corrosion*, vol. 2, no. 2, pp. 1–7, 2016, doi: 10.1007/s40735-016-0042-3.
- [12] K. Wang *et al.*, “Microstructural Evolution and Mechanical Properties of 7075 Aluminium Alloy during Semi-Solid Compression Deformation,” *Crystals*, vol. 12, no. 8, 2022, doi: 10.3390/cryst12081119.
- [13] J. feng LI, Z. wei PENG, C. xing LI, Z. qiang JIA, W. jing CHEN, and Z. qiao ZHENG, “Mechanical properties, corrosion behaviors and microstructures of 7075 aluminium alloy with various aging treatments,” *Trans. Nonferrous Met. Soc. China (English Ed.)*, vol. 18, no. 4, pp. 755–762, 2008, doi: 10.1016/S1003-6326(08)60130-2.
- [14] R. S. Neves, D. P. B. Silva, and A. J. Motheo, “Corrosion Protection of AA7075 Aluminium Alloy by Trimethoxy-Silanes Self-Assembled Monolayers,” *ISRN Electrochem.*, vol. 2013, no. i, pp. 1–9, 2013, doi: 10.1155/2013/142493.
- [15] M. Fousova, V. Valesova, and D. Vojtech, “Corrosion of 3D-printed AlSi9Cu3Fe alloy,” *Manuf. Technol.*, vol. 19, no. 1, pp. 29–36, 2019, doi: 10.21062/ujep/240.2019/a/1213-2489/mt/19/1/29.
- [16] E. Beltowska-Lehman, A. Bigos, P. Indyka, and M. Kot, “Electrodeposition and characterisation of nanocrystalline Ni-Mo coatings,” *Surf. Coatings Technol.*, vol. 211, pp. 67–71, 2012, doi: 10.1016/j.surfcoat.2011.10.011.
- [17] M. P. Martínez-Viademonte, S. T. Abrahami, T. Hack, M. Burchardt, and H. Terry, “A review on anodizing of aerospace aluminum alloys for corrosion protection,” *Coatings*, vol. 10, no. 11, pp. 1–30, 2020, doi: 10.3390/coatings10111106.



- [18] M. Williams, "An Alternative To Chromates for Corrosion Protection for Aluminum Alloys," p. 82, 2011, [Online]. Available: <http://digitalcommons.uri.edu/theses/125>
- [19] P. Gadhari and P. Sahoo, "Improvement of corrosion resistance of Ni-P-Al<sub>2</sub>O<sub>3</sub> composite coating by optimizing process parameters using potentiodynamic polarization test," *Port. Electrochim. Acta*, vol. 32, no. 2, pp. 137–156, 2014, doi: 10.4152/pea.201402137.
- [20] M. Hong Seo, J. Soo Kim, W. Suk Hwang, D. Jin Kim, S. Sik Hwang, and B. Sun Chun, "Characteristics of Ni-P alloy electrodeposited from a sulfamate bath," *Surf. Coatings Technol.*, vol. 176, pp. 135–140, 2004, doi: 10.1016/S0257-8972.
- [21] D. H. Jeong, U. Erb, K. T. Aust, and G. Palumbo, "The relationship between hardness and abrasive wear resistance of electrodeposited nanocrystalline Ni-P coatings," *Scr. Mater.*, vol. 48, no. 8, pp. 1067–1072, 2003, doi: 10.1016/S1359-6462(02)00633-4.
- [22] T. Morikawa, "Electrodeposition of Ni-P alloys from Ni-citrate bath," vol. 42, no. 1, pp. 1–4, 1997.
- [23] J. N. Balaraju and K. S. Rajam, "Electroless deposition and characterization of high phosphorus Ni-P-Si<sub>3</sub>N<sub>4</sub> composite coatings," *Int. J. Electrochem. Sci.*, vol. 2, no. 10, pp. 747–761, 2007, doi: 10.1016/s1452-3981(23)17109-4.
- [24] J. N. Balaraju, V. Ezhil Selvi, and K. S. Rajam, "Electrochemical behavior of low phosphorus electroless Ni-P-Si<sub>3</sub>N<sub>4</sub> composite coatings," *Mater. Chem. Phys.*, vol. 120, no. 2–3, pp. 546–551, 2010, doi: 10.1016/j.matchemphys.2009.11.047.
- [25] V. B. Chintada, R. Koon, and M. V. A. Raju Bahubalendruni, "State of Art Review on Nickel-Based Electroless Coatings and Materials," *J. Bio- Tribo-Corrosion*, vol. 7, no. 4, pp. 1–14, 2021, doi: 10.1007/s40735-021-00568-7.
- [26] S. Ranganatha, T. V. Venkatesha, and K. Vathsala, "Development of high performance electroless Ni-P-HNT composite coatings," *Appl. Surf. Sci.*, vol. 263, pp. 149–156, 2012, doi: 10.1016/j.apsusc.2012.09.020.
- [27] S. Mohan Kumar, R. Pramod, M. E. Shashi Kumar, and H. K. Govindaraju, "Evaluation of fracture toughness and mechanical properties of aluminum alloy 7075, T6 with nickel

- coating,” *Procedia Eng.*, vol. 97, pp. 178–185, 2014, doi: 10.1016/j.proeng.2014.12.240.
- [28] O. E. ASHIBUDIKE and B. U. OREKO, “Biochemical Synthesis and Characterisation of Cobalt Nanoparticles,” *Eur. J. Mater. Sci. Eng.*, vol. 8, no. 2, pp. 86–95, 2023, doi: 10.36868/ejmse.2023.08.02.086.
- [29] J. N. Balaraju, T. S. N. Sankara Narayanan, and S. K. Seshadri, “Structure and phase transformation behaviour of electroless Ni-P composite coatings,” *Mater. Res. Bull.*, vol. 41, no. 4, pp. 847–860, 2006, doi: 10.1016/j.materresbull.2005.09.024.
- [30] M. Czagány, P. Baumli, and G. Kaptay, “The influence of the phosphorous content and heat treatment on the nano-micro-structure, thickness and micro-hardness of electroless Ni-P coatings on steel,” *Appl. Surf. Sci.*, vol. 423, pp. 160–169, 2017, doi: 10.1016/j.apsusc.2017.06.168.
- [31] A. You, M. Be, and I. In, “Chemical nature of phosphorus in Ni–P deposits □,” vol. 4835, no. July, pp. 4834–4835, 2023.
- [32] R. A. Shakoor and A. Bahgat Radwan, “Remarkable improvement in properties of NI-B coatings by the addition of mixed oxide nanoparticles,” *Mater. Sci. Technol. Conf. Exhib. 2015, MS T 2015*, vol. 1, no. 9, pp. 171–178, 2015, doi: 10.1016/S1452-3981(23)17370-6.
- [33] W. Sha, X. Wu, and K. G. Keong, “Crystallisation of nickel–phosphorus (Ni–P) deposits with high phosphorus content,” *Electroless Copp. Nickel–Phosphorus Plat.*, pp. 141–162, 2011, doi: 10.1533/9780857090966.2.141.
- [34] A. Sadeghzadeh-Attar, G. AyubiKia, and M. Ehteshamzadeh, “Improvement in tribological behavior of novel sol-enhanced electroless Ni-P-SiO<sub>2</sub> nanocomposite coatings,” *Surf. Coatings Technol.*, vol. 307, pp. 837–848, 2016, doi: 10.1016/j.surfcoat.2016.10.026.
- [35] O. Fayyaz *et al.*, “Enhancement of mechanical and corrosion resistance properties of electrodeposited Ni–P–TiC composite coatings,” *Sci. Rep.*, vol. 11, no. 1, pp. 1–16, 2021, doi: 10.1038/s41598-021-84716-6.
- [36] K. Shahzad *et al.*, “Effect of concentration of TiC on the properties of pulse electrodeposited Ni–P–TiC nanocomposite coatings,” *Ceram. Int.*, vol. 47, no. 13, pp. 19123–19133, 2021,

doi: 10.1016/j.ceramint.2021.03.259.

- [37] I. Fatima, O. Fayyaz, M. M. Yusuf, A. Al Ashraf, and R. A. Shakoor, “Enhanced electrochemical and mechanical performance of BN reinforced Ni-P based nanocomposite coatings,” *Diam. Relat. Mater.*, vol. 130, no. August, p. 109454, 2022, doi: 10.1016/j.diamond.2022.109454.
- [38] R. Taheri, I. N. A. Oguocha, and S. Yannacopoulos, “The tribological characteristics of electroless NiP coatings,” *Wear*, vol. 249, no. 5–6, pp. 389–396, 2001, doi: 10.1016/S0043-1648(01)00539-7.
- [39] M. Buchtík, M. Krystýnová, J. Másilko, and J. Wasserbauer, “The effect of heat treatment on properties of Ni-P coatings deposited on a AZ91 magnesium alloy,” *Coatings*, vol. 9, no. 7, 2019, doi: 10.3390/coatings9070461.
- [40] E. M. Fayyad *et al.*, “Synthesis, characterization, and application of novel Ni-P-carbon nitride nanocomposites,” *Coatings*, vol. 8, no. 1, pp. 1–13, 2018, doi: 10.3390/coatings8010037.
- [41] O. Fayyaz, A. Bahgat Radwan, M. H. Sliem, A. M. Abdullah, A. Hasan, and R. A. Shakoor, “Investigating the Properties of Electrodeposited of Ni-P-ZrC Nanocomposite Coatings,” *ACS Omega*, vol. 6, no. 49, pp. 33310–33324, 2021, doi: 10.1021/acsomega.1c03117.
- [42] M. H. Sliem *et al.*, “Enhanced mechanical and corrosion protection properties of pulse electrodeposited NiP-ZrO<sub>2</sub> nanocomposite coatings,” *Surf. Coatings Technol.*, vol. 403, no. June, p. 126340, 2020, doi: 10.1016/j.surfcoat.2020.126340.
- [43] A. Bahgat Radwan *et al.*, “Properties enhancement of Ni-P electrodeposited coatings by the incorporation of nanoscale Y<sub>2</sub>O<sub>3</sub> particles,” *Appl. Surf. Sci.*, vol. 457, pp. 956–967, 2018, doi: 10.1016/j.apsusc.2018.06.241.
- [44] M. H. Sliem *et al.*, “Enhanced mechanical and corrosion protection properties of pulse electrodeposited NiP-ZrO<sub>2</sub> nanocomposite coatings,” *Surf. Coatings Technol.*, vol. 403, no. August, p. 126340, 2020, doi: 10.1016/j.surfcoat.2020.126340.